Chapter 6
Magnetism and Conduction

Abstract After the description of the electron hopping in systems where not all the magnetic centers have the same number of unpaired electrons, a short account is given of the double exchange mechanism in mixed-valence systems. Although this phenomenon can certainly be found in transition metal complexes, it is more common to happen in doped systems in the solid state. Therefore, the second part of this chapter introduces the basics of the quantum chemical approach to magnetic interactions in extended systems. The embedded cluster approach will be contrasted against band structure calculations. Thereafter, some concepts will be introduced that are widely used in the condensed matter physics community. We do not give a full description of all the magnetic phenomena in solid state compounds but rather help the reader with a quantum chemical background to find its way in the rich literature on this topic.

6.1 Electron Hopping

In all the magnetic systems described so far the number of magnetic orbitals was equal to the number of unpaired electrons. These systems are generally known as half-filled systems and the price (in terms of energy) to move an electron from one site to another is proportional to the on-site repulsion parameter U. Since this parameter is in general huge in comparison to the magnetic interactions, the electrons are considered to be immobile or in other words, trapped on the magnetic sites. The situation changes drastically when the number of electrons in the magnetic orbitals is no longer equal to the number of magnetic orbitals, that is when the system is doped with electrons (more electrons than magnetic orbitals) or doped with holes (less electrons than magnetic orbitals). In these systems, the electron is no longer necessarily trapped and can move from site to site under certain circumstances that will be described below. A commonly used classification of magnetic compounds by the degree of electron mobility was given by Robin and Day [1], who divided the so-called mixed valence compounds into three groups. Class I contains all the compounds where the magnetic centers have different oxidation states but the electrons are nevertheless trapped. Class III is quite the opposite; the magnetic centers have formally a distinct oxidation state

C. Graaf and R. Broer, *Magnetic Interactions in Molecules and Solids*,
Theoretical Chemistry and Computational Modelling,
DOI 10.1007/978-3-319-22951-5_6

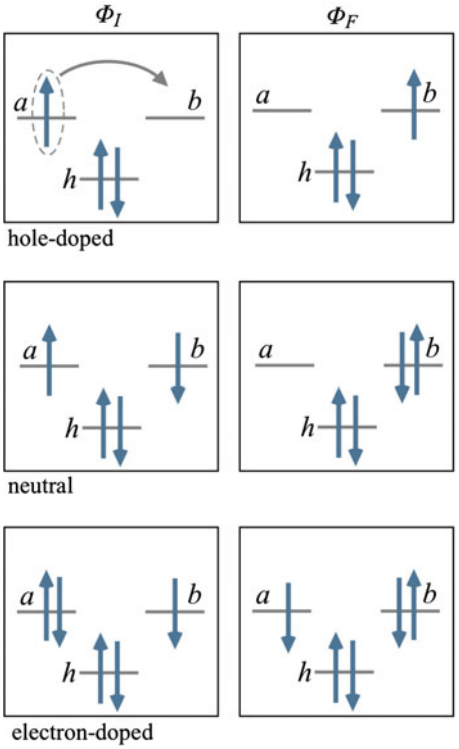

Fig. 6.1 Initial and final states of electron hopping processes in hole-doped, neutral and electron-doped magnetic systems

but the electrons are completely delocalized and in practice all magnetic centers share the same average oxidation, often a non-integer number. In between, one finds the probably most interesting case of Class II compounds. There is a certain degree of localization but the hopping of an electron from one site to a neighbouring one has a low energy barrier and occurs frequently.

In the background of a collection of inactive doubly occupied orbitals *h*, three different scenarios can be envisaged to describe electron hopping processes. Figure 6.1 illustrates these scenarios and from top to bottom we recognize the hopping process from a singly occupied orbital to an empty orbital; from a singly occupied to another singly occupied orbital; and from a doubly occupied (filled) to a singly occupied orbital. Taking the system in the middle as reference *neutral* system, the upper part of the figure is indicative for electron hopping in a hole-doped (or electron-ionized) system, while the bottom illustrates the hopping in an electron-doped system. In this case the process is often interpreted in terms of hole mobility, where the figure illustrates how a hole on site B moves to site A.

The probability for these hopping processes is normally condensed into a single parameter referred to as t_{ab}, but V_{ab} and β (Hückel theory) are also used. Intuitively one would say that the hopping parameter is the same for all three processes, since one electron moves from a to b, while the rest of the occupations stay the same in all cases. But the calculation of the $\langle \Phi_I | \hat{H} | \Phi_F \rangle$ matrix element shows that this is not exactly the case. The interaction matrix elements of the initial and final states are easily determined with the Slater–Condon rules. In the first case, the hopping of an electron to an empty orbital is defined by

$$\Phi_I = |h\bar{h}a| \qquad \Phi_F = |h\bar{h}b|$$
$$t_{ab}^{+} = \langle \Phi_I | \hat{H} | \Phi_F \rangle = \sum_h \langle ah | \frac{1}{r_{12}} | bh \rangle + \langle a | \hat{h} | b \rangle \tag{6.1a}$$

where a and b are (orthogonal) atomic-like orbitals centered on the centers A and B and h is one of the inactive doubly occupied orbitals. The sum runs over all the inactive orbitals. In the second scenario, the initial and final states and their matrix element are

$$\Phi_I = |h\bar{h}a\bar{b}| \qquad \Phi_F = |h\bar{h}b\bar{b}|$$
$$t_{ab}^{0} = \langle \Phi_I | \hat{H} | \Phi_F \rangle = \sum_h \langle ah | \frac{1}{r_{12}} | bh \rangle + \langle a | \hat{h} | b \rangle + \langle ab | \frac{1}{r_{12}} | bb \rangle \tag{6.1b}$$

and finally, the process on the bottom of the figure from doubly to singly occupied is described by

$$\Phi_I = |h\bar{h}a\bar{a}b| \qquad \Phi_F = |h\bar{h}ab\bar{b}|$$
$$t_{ab}^{-} = \langle \Phi_I | \hat{H} | \Phi_F \rangle = \sum_h \langle ah | \frac{1}{r_{12}} | bh \rangle + \langle a | \hat{h} | b \rangle + \langle ab | \frac{1}{r_{12}} | bb \rangle + \langle aa | \frac{1}{r_{12}} | ba \rangle \tag{6.1c}$$

The contribution of the inactive doubly occupied orbitals is the same in the three cases as is the one-electron term h_{ab}. However, the appearance of two-electron integrals for those cases with more than one electron in the magnetic orbitals introduces differences in the interaction matrix elements.

Numerical estimates of the hopping parameter are relatively easy to obtain with the different computational schemes discussed in Chap. 4. Starting with t_{ab}^{+} in a centrosymmetric two-site system, two electronic states can be defined with doublet spin coupling

$$D_1 = |h\bar{h}g| \qquad D_2 = |h\bar{h}u| \tag{6.2}$$

with g and u the bonding and anti-bonding combinations of the local orbitals a and b. The energy of the two doublets is

$$\begin{aligned} E(D_1) &= \langle h\bar{h}g|\hat{H}|h\bar{h}g\rangle = \frac{1}{2}\langle h\bar{h}(a+b)|\hat{H}|h\bar{h}(a+b)\rangle \\ &= \frac{1}{2}\big(\langle h\bar{h}a|\hat{H}|h\bar{h}a\rangle + 2\langle h\bar{h}a|\hat{H}|h\bar{h}b\rangle + \langle h\bar{h}b|\hat{H}|h\bar{h}b\rangle\big) \qquad (6.3) \\ E(D_2) &= \langle h\bar{h}u|\hat{H}|h\bar{h}u\rangle = \frac{1}{2}\langle h\bar{h}(a-b)|\hat{H}|h\bar{h}(a-b)\rangle \\ &= \frac{1}{2}\big(\langle h\bar{h}a|\hat{H}|h\bar{h}a\rangle - 2\langle h\bar{h}a|\hat{H}|h\bar{h}b\rangle + \langle h\bar{h}b|\hat{H}|h\bar{h}b\rangle\big) \qquad (6.4) \end{aligned}$$

Combining the energy difference of the two doublets

$$\Delta E_{12} = E(D_1) - E(D_2) = 2\langle h\bar{h}a|\hat{H}|h\bar{h}b\rangle \qquad (6.5)$$

with the definition given in Eq. 6.1a, the hopping parameter can be calculated by

$$t_{ab}^{+} = \frac{1}{2}\Delta E_{12} \qquad (6.6)$$

In practice, an effective hopping parameter can be obtained from accurate *ab initio* energies for the two doublets. For non-centrosymmetric systems, the calculation is slightly more involved. The two doublets are now defined as

$$D_1 = c_1|h\bar{h}a| + c_2|h\bar{h}b| \qquad D_2 = c_2|h\bar{h}a| - c_1|h\bar{h}b| \qquad (6.7)$$

and the energy difference is

$$\Delta E_{12} = (c_1^2 - c_2^2)(H_{aa} - H_{bb}) + 4c_1c_2H_{ab} \qquad (6.8)$$

with $H_{ij} = \langle h\bar{h}i|\hat{H}|h\bar{h}j\rangle$. This leads to the following expression for t_{ab}^{+}

$$t_{ab}^{+} = \frac{\Delta E_{12} - (c_1^2 - c_2^2)(H_{aa} - H_{bb})}{4c_1c_2} \qquad (6.9)$$

To determine t, the energy difference is no longer sufficient and information is required from the wave function. The magnetic orbitals have to be expressed in orthogonal atomic-like orbitals and the wave functions projected on the model space $\{|h\bar{h}a|, |h\bar{h}b|\}$. After orthonormalization, a numerical 2×2 effective Hamiltonian can be constructed

$\hat{H}^{eff}$	$\lvert h\bar{h}a\rangle$	$\lvert h\bar{h}b\rangle$
$\langle h\bar{h}a\rvert$	H_{aa}	t_{ab}^{+}
$\langle h\bar{h}b\rvert$	t_{ab}^{+}	H_{bb}

and the hopping parameter can be directly determined from the off-diagonal matrix element.

6.1 Show that the expression of t_{ab}^{+} for the non-centrosymmetric case reduces to $\Delta E_{12}/2$ for a centrosymmetric system.

The determination of t_{ab}^{0} has already been discussed in Sect. 5.2. It requires the construction of a 4×4 effective Hamiltonian with a basis of two neutral and two ionic determinants. The hopping integral is defined as the matrix element between neutral and ionic determinants. The calculation of t_{ab}^{-} is analogous to the procedure for estimating t_{ab}^{+}. The two doublets that can be defined in a centrosymmetric complex with three electrons in the two magnetic orbitals g and u (omitting $h\bar{h}$ for simplicity)

$$D_1 = |gu\bar{u}| \qquad D_2 = |g\bar{g}u| \tag{6.10}$$

are re-expressed in the orthogonal atomic-like orbitals a and b

$$\begin{aligned} D_1 &= \frac{1}{2\sqrt{2}}|(a+b)(a-b)(\bar{a}-\bar{b})| = \frac{1}{2\sqrt{2}}|-ab\bar{a}+ab\bar{b}+ba\bar{a}-ba\bar{b}| \\ &= \frac{1}{\sqrt{2}}(|ab\bar{b}|+|a\bar{a}b|) \end{aligned} \tag{6.11a}$$

$$\begin{aligned} D_2 &= \frac{1}{2\sqrt{2}}|(a+b)(\bar{a}+\bar{b})(a-b)| = \frac{1}{2\sqrt{2}}|-a\bar{a}b-a\bar{b}b+b\bar{a}a+b\bar{b}a| \\ &= \frac{1}{\sqrt{2}}(|ab\bar{b}|-|a\bar{a}b|) \end{aligned} \tag{6.11b}$$

The energies of the two states are

$$\begin{aligned} E_1 &= \frac{1}{2}\langle ab\bar{b}+a\bar{a}b|\hat{H}|ab\bar{b}+a\bar{a}b\rangle \\ &= \frac{1}{2}\left[\langle ab\bar{b}|\hat{H}|ab\bar{b}\rangle + 2\langle ab\bar{b}|\hat{H}|a\bar{a}b\rangle + \langle a\bar{a}b|\hat{H}|a\bar{a}b\rangle\right] \end{aligned} \tag{6.12a}$$

$$\begin{aligned} E_2 &= \frac{1}{2}\langle ab\bar{b}-a\bar{a}b|\hat{H}|ab\bar{b}-a\bar{a}b\rangle \\ &= \frac{1}{2}\left[\langle ab\bar{b}|\hat{H}|ab\bar{b}\rangle - 2\langle ab\bar{b}|\hat{H}|a\bar{a}b\rangle + \langle a\bar{a}b|\hat{H}|a\bar{a}b\rangle\right] \end{aligned} \tag{6.12b}$$

and t_{ab}^{-} can again be calculated from the energy difference of the two doublets, see Eq. 6.10:

$$t_{ab}^{-} = \frac{1}{2}\Delta E_{12} = \langle ab\bar{b}|\hat{H}|a\bar{a}b\rangle \tag{6.13}$$

6.2 Double Exchange

The concept of *double exchange* was introduced by Zener in the 1950s to explain the sudden drop in the resistance of certain manganites when an external magnetic field was applied [2]. The manganese ions in these compounds have either three or four unpaired electrons in the $3d$-shell; three electrons in t_{2g}-like orbitals and the fourth electron in an e_g-like orbital. Electron hopping in such compounds takes place in the presence of other unpaired electrons and depending on the inter-site spin coupling of the t_{2g} electrons, the e_g electron has more or less probability to hop to a neighboring site. Assume that the antiferromagnetic coupling dominates in the absence of an external magnetic field. As shown in the upper part of Fig. 6.2, the electron hopping leads to a state that does not have the maximum spin on the center that receives the electron, whereas maximum spin coupling at one site is preferred as stated by Hund's rule. By applying a sufficiently large external magnetic field, the spins on all centers can be forced in a ferromagnetic alignment. In such a case, see the lower part of the figure, the electron hopping creates a high-spin state on the receiving center, which corresponds to the local ground state and this is more favorable for electron mobility, i.e. an external magnetic field can drastically lower the resistance to electric conductance.

The effectiveness of the electron hopping between two metal centers separated by a closed-shell ion, typically O^{2-}, inspired Zener to introduce the concept of *double exchange* illustrated in Fig. 6.3. The simultaneous hopping process of an electron with α-spin from the first metal center to the O^{2-} ion and from this O^{2-} ion to the second metal center was held responsible for the hopping. Contrary to the superexchange described in Fig. 5.4, the double exchange only involves electrons of the same spin. Therefore, the intuitive picture is that since the electron transfers can take place simultaneously, in contrast to the superexchange, the double exchange hopping is very efficient.

This simple electron hopping explanation has later been revised to incorporate the strong electron-phonon coupling caused by the Jahn-Teller splitting of the Mn^{3+} ions. The conduction is due to the hopping of a *magnetic polaron* rather than a bare electron [3].

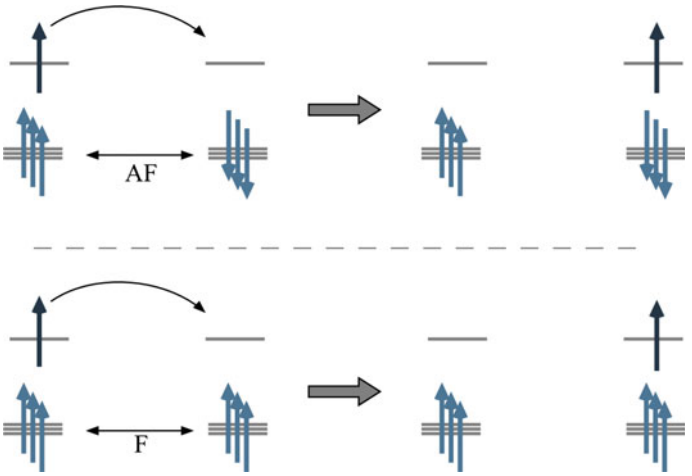

Fig. 6.2 Schematic explanation for the spin dependence of the hopping probability of the extra electron in a background of unpaired electrons

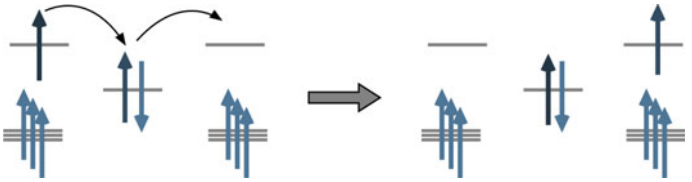

Fig. 6.3 Double exchange mechanism proposed by Zener consisting in the simultaneous hopping of an electron from center 1 to the bridge and from the bridge to metal 2

Fig. 6.4 Simple model to describe electron hopping in the background of unpaired electrons, the orbitals are mutually orthogonal

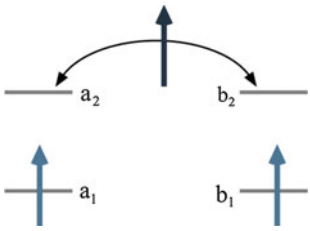

A rigorous description of electron hopping in the presence of other unpaired electrons can be written down for the simple model system defined in Fig. 6.4. The two electrons in the a_1 and b_1 orbitals provide a static background of unpaired electrons for the mobile electron in the a_2 b_2 channel. Choosing $M_S = \frac{1}{2}$, there are 24 ways to distribute the three electrons over the four orbitals, but only six of them

are essential to the basic description of the hopping process of the electron between the a_2 and b_2 orbitals. The six determinants are

$$\begin{aligned} \Phi_1 &= |a_1 b_1 \overline{a}_2| & \Phi_4 &= |a_1 b_1 \overline{b}_2| \\ \Phi_2 &= |a_1 \overline{b}_1 a_2| & \Phi_5 &= |\overline{a}_1 b_1 b_2| \\ \Phi_3 &= |\overline{a}_1 b_1 a_2| & \Phi_6 &= |a_1 \overline{b}_1 b_2| \end{aligned} \tag{6.14}$$

6.2 Find the four determinants (or linear combinations of determinants) that represent a triplet spin coupling of the electrons on center a or b. What is the spin coupling of the other two (linear combinations) of determinants? What do you expect for the relative energies of the two groups?

The interaction matrix elements are readily written down using the Slater–Condon rules given in Chap. 1. We will work out three examples and leave the others as exercise to the reader.

$$\begin{aligned} \langle \Phi_1 | \hat{H} | \Phi_1 \rangle = \langle a_1 b_1 \overline{a}_2 | \hat{H} | a_1 b_1 \overline{a}_2 \rangle &= \langle a_1 | \hat{h} | a_1 \rangle + \langle b_1 | \hat{h} | b_1 \rangle + \langle a_2 | \hat{h} | a_2 \rangle \\ &+ \langle a_1 b_1 | \frac{1 - \hat{P}_{12}}{r_{12}} | a_1 b_1 \rangle + \langle a_1 \overline{a}_2 | \frac{1 - \hat{P}_{12}}{r_{12}} | a_1 \overline{a}_2 \rangle + \langle b_1 \overline{a}_2 | \frac{1 - \hat{P}_{12}}{r_{12}} | b_1 \overline{a}_2 \rangle \end{aligned} \tag{6.15}$$

The two-electron part becomes

$$\begin{aligned} &\langle a_1 b_1 | \frac{1}{r_{12}} | a_1 b_1 \rangle - \langle a_1 b_1 | \frac{1}{r_{12}} | b_1 a_1 \rangle + \langle a_1 a_2 | \frac{1}{r_{12}} | a_1 a_2 \rangle + \langle b_1 a_2 | \frac{1}{r_{12}} | b_1 a_2 \rangle \\ &= J_{a_1 b_1} + J_{a_1 a_2} + J_{b_1 a_2} - K_{a_1 b_1} \end{aligned} \tag{6.16}$$

The one-electron part and the Coulomb integrals J_{xy} are common to all diagonal matrix elements and the sum of these terms can be taken as the zero of energy. Then, the matrix element $\langle \Phi_1 | \hat{H} | \Phi_1 \rangle$ reduces to the exchange integral $-K_{a_1 b_1}$. Likewise, the diagonal elements involving Φ_2 and Φ_3 reduce to $K_{a_1 a_2}$ and to 0, respectively. The off-diagonal matrix element between Φ_2 and Φ_3 is relatively simple

$$\begin{aligned} \langle \Phi_2 | \hat{H} | \Phi_3 \rangle = \langle a_1 \overline{b}_1 a_2 | \hat{H} | \overline{a}_1 b_1 a_2 \rangle &= \langle a_1 \overline{b}_1 | \frac{1 - \hat{P}_{12}}{r_{12}} | \overline{a}_1 b_1 \rangle \\ &= -\langle a_1 b_1 | \frac{1}{r_{12}} | b_1 a_1 \rangle = -K_{a_1 b_1} \end{aligned} \tag{6.17}$$

but the matrix element between Φ_1 and Φ_4 is slightly more involved

$$\langle \Phi_1|\hat{H}|\Phi_4\rangle = \langle a_1 b_1 \bar{a}_2|\hat{H}|a_1 b_1 \bar{b}_2\rangle = \langle a_2|\hat{h}|b_2\rangle + \langle a_1\bar{a}_2|\frac{1-\hat{P}_{12}}{r_{12}}|a_1\bar{b}_2\rangle$$
$$+ \langle b_1\bar{a}_2|\frac{1-\hat{P}_{12}}{r_{12}}|b_1\bar{b}_2\rangle = \langle a_2|\hat{h}|b_2\rangle + \langle a_1 a_2|\frac{1}{r_{12}}|a_1 b_2\rangle + \langle b_1 a_2|\frac{1}{r_{12}}|b_1 b_2\rangle \tag{6.18}$$

where the two-electron integrals cannot be written as Coulomb or exchange integrals. The sum of the three terms can be considered as the hopping parameter t, similar to the expressions given in Eqs. 6.1b and 6.1c. The complete interaction matrix is

$\hat{H}$	$\|\Phi_1\rangle$	$\|\Phi_2\rangle$	$\|\Phi_3\rangle$	$\|\Phi_4\rangle$	$\|\Phi_5\rangle$	$\|\Phi_6\rangle$
$\langle\Phi_1\|$	$-K'$	0	$-K$	t	0	0
$\langle\Phi_2\|$	0	$-K$	$-K'$	0	0	t
$\langle\Phi_3\|$	$-K$	$-K'$	0	0	t	0
$\langle\Phi_4\|$	t	0	0	$-K'$	0	$-K$
$\langle\Phi_5\|$	0	0	t	0	$-K$	$-K'$
$\langle\Phi_6\|$	0	t	0	$-K$	$-K'$	0

$K = K_{a_1 a_2} = K_{b_1 b_2}$ is the on-site exchange interaction and $K' = K_{a_1 b_1}$ is the intersite exchange. Two approximations have been made to obtain this matrix. In the first place, it is assumed that $K_{a_i b_j}$ with $i \neq j$ can be neglected. Furthermore, we assume that the effect of the so-called singlet displacement operator is small enough to be omitted. The action of this operator is illustrated in Fig. 6.5 and transforms Φ_1 into Φ_5 or Φ_6, and Φ_4 into Φ_2 or Φ_3.

6.3 Show that the other zeros in the matrix are real zeros and not due to any additional approximation. Explain why in the Hamiltonian matrix $H_{11} = H_{44}$, $H_{22} = H_{55}$, $H_{33} = H_{66}$, and $H_{13} = H_{46}$.

The diagonalization of the matrix yields six eigenstates, two quartets and four doublets with the following energies after shifting all states with $K + K'$ to let the zero of energy coincide with the average energy of the quartet states

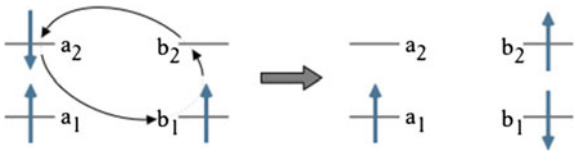

Fig. 6.5 Action of the singlet displacement operator

$$E(Q_{1,2}) = \pm t \tag{6.19}$$

$$E(D_{1,2}) = K + K' - \sqrt{K^2 + t(t \pm K) + K'^2 - K'(K \pm 2t)} \tag{6.20}$$

$$E(D_{3,4}) = K + K' + \sqrt{K^2 + t(t \pm K) + K'^2 - K'(K \pm 2t)} \tag{6.21}$$

The first two doublets are dominated by the CSFs with triplet coupling on center a or b, and hence, much lower in energy than the third and fourth doublets with local singlet coupling. The latter states are similar to the non-Hund states invoked to explain the deviations to the regular Heisenberg pattern in Sect. 5.4. The quartet states are in-phase and out-of-phase linear combinations of the high spin coupled determinants with the extra electron on center a or center b, which is most conveniently seen in the $M_S = 3/2$ components of these states.

$$Q_1(M_S = 3/2) = \frac{1}{\sqrt{2}}\big(a_1 b_1 a_2 + a_1 b_1 b_2\big) \tag{6.22}$$

$$Q_2(M_S = 3/2) = \frac{1}{\sqrt{2}}\big(a_1 b_1 a_2 - a_1 b_1 b_2\big) \tag{6.23}$$

In the simplest description of the hopping, the on-site exchange integral is assumed to be so large in comparison to the other parameters that the doublet states dominated by the non-Hund determinants are not relevant and the energy of the lower doublet states can be simplified to

$$E(D_{1,2}) = K - \sqrt{K^2} + \frac{1}{2}\frac{t(t \pm K) + K'^2 - K'(K \pm 2t)}{\sqrt{K^2}} = \pm\frac{1}{2}t + \frac{3}{2}K' \tag{6.24}$$

using the Taylor expansion $\sqrt{p+q} = \sqrt{p} + \frac{1}{2}q/\sqrt{p} + \ldots$ and neglecting all terms proportional to K^{-1} because K is very large in comparison to t and K'. A general expression for any number of unpaired electrons within this approximation is

$$E(S) = \pm t\frac{S + 1/2}{S_{max} + 1/2} + \frac{1}{2}\big(S_{max}(S_{max} + 1) - S(S + 1)\big)K' \tag{6.25}$$

Recalling that the exchange parameters $K_{a_1 b_2}$ and $K_{a_2 b_1}$ have been neglected, the K' parameter plays exactly the same role as the Heisenberg J in the description of Girerd, who included the magnetic coupling between the two sites with S_A and S_B spin moments in the description of the double exchange. Then the equation can also be written in a more familiar form [4].

$$E(S) = \pm t\frac{S + 1/2}{S_{max} + 1/2} + \frac{1}{2}J\big(S_{max}(S_{max} + 1) - S(S + 1)\big) \tag{6.26}$$

It is interesting to see that even when the intersite interaction is completely neglected by putting J (or K') to zero, the hopping process forces the system into the ferromagnetic state. Only when J is very strongly antiferromagnetic and t relatively small, one may expect a low-spin ground state. In the more common case that t dominates, we see that the transfer integral is reduced by the factor $(S + 1/2)/(S_{max} + 1/2)$.

An important aspect of the physics of double exchange compounds is the interaction between the electron distribution and the movement of the nuclei by vibronic coupling in complexes or electron-phonon interaction in extended systems. This goes beyond the scope of this book and we refer the interested reader to Ref. [5] for further reading.

Semi-classical description of the double exchange: The first description of the double exchange by Zener [2] gave a simple (yet convincing) explanation of the strong dependence of the electric resistivity on the strength of the external magnetic field. The model only considers the hopping parameter t and assumes that the intra-atomic exchange integral is infinitely large, which makes that the electron can only move through the material when all spins at the magnetic sites are ferromagnetically aligned. A more detailed description was given by Anderson and Hasegawa [6], who derived the first right-hand-side term of Eq. 6.26. Here, we will review the semi-classical description of these authors to illustrate the concept of spin dependent hopping which is the basis of the Goodenough–Kanamori rules treated in the Sect. 6.4.

The Anderson–Hasegawa model describes the electron transfer from site A to B in the field of the spin moments $\mathbf{S}_A$ and $\mathbf{S}_B$, which are described as classical vectors. The spin moments are not necessarily co-linear but have an angle θ. The justification for this semi-classical description is that for large spin moments the quantum mechanical description converges with the classical one. Being applied to describe the electron hopping in manganites, this approximation is not as severe due to the relatively large spin moment on the manganese ions. Since the magnetic axes frames on site A and B do not have the same orientation, the basis of spin functions of site A (α and β) has to be expressed in terms of the basis of spin functions of site B (α' and β').

$$\alpha = \cos(\theta/2)\alpha' + \sin(\theta/2)\beta' \tag{6.27a}$$

$$\beta = -\sin(\theta/2)\alpha' + \cos(\theta/2)\beta' \tag{6.27b}$$

The basis functions of this semi-classical model are $\phi_1 = a\alpha$, $\phi_2 = a\beta$, $\phi_3 = b\alpha'$ and $\phi_4 = b\beta'$, where a and b define the spatial part of the orbitals that carry the mobile electron. The following definition of the interaction for $\theta = 0$ is used

$$\langle a\alpha|\hat{H}|b\alpha\rangle = \tau \tag{6.28a}$$

$$\langle a\alpha|\hat{H}|b\beta\rangle = 0 \tag{6.28b}$$

and for $\theta \neq 0$, slightly more elaborated expressions are obtained

$$\langle a\alpha|\hat{H}|b\alpha'\rangle = \langle a\big(\cos(\theta/2)\alpha' + \sin(\theta/2)\beta'\big)|\hat{H}|b\alpha'\rangle = \tau\cos(\theta/2) \tag{6.28c}$$

$$\langle a\alpha|\hat{H}|b\beta'\rangle = \tau\sin(\theta/2) \tag{6.28d}$$

$$\langle a\beta|\hat{H}|b\alpha'\rangle = -\tau\sin(\theta/2) \tag{6.28e}$$

$$\langle a\beta|\hat{H}|b\beta'\rangle = \tau\cos(\theta/2) \tag{6.28f}$$

The spin moment of $a\alpha$ and $b\alpha'$ is parallel to $\mathbf{S}_A$ and $\mathbf{S}_B$, respectively. In the simplest description, the energy of these states with respect to the ones with antiparallel alignment ($a\beta$ and $b\beta'$) is given by the number of exchange interactions between the extra electron and the electrons that give rise to the background spin moments S_A and S_B.

$$E_{1,3} = -K \cdot 2S_{A,B} \qquad E_{2,4} = 0 \tag{6.29}$$

However, in a formalism with correct spin eigenfunctions the energies become

$$E_{1,3} = -K(S_{A,B} + 1) \qquad E_{2,4} = +KS_{A,B} \tag{6.30}$$

6.4 Consider a magnetic site with a $S = 1$ background spin moment (triplet coupled electrons in φ_1 and φ_2) and an electron in φ_3 that can hop to neighboring centers. Calculate the energies of $|\varphi_1\varphi_2\varphi_3|$, $|\varphi_1\varphi_2\overline{\varphi}_3|$ and the CSF for the doublet with triplet coupling for φ_1 and φ_2 and compare to the Eqs. 6.29 and 6.30.

With these ingredients the matrix representation of the model Hamiltonian can be constructed

	$\lvert a\alpha\rangle$	$\lvert a\beta\rangle$	$\lvert b\alpha'\rangle$	$\lvert b\beta'\rangle$
$\langle a\alpha\rvert$	$-K(S_A+1)$	0	$\tau\cos(\theta/2)$	$\tau\sin(\theta/2)$
$\langle b\beta\rvert$	0	KS_A	$-\tau\sin(\theta/2)$	$\tau\cos(\theta/2)$
$\langle a\alpha'\rvert$	$\tau\cos(\theta/2)$	$-\tau\sin(\theta/2)$	$-K(S_B+1)$	0
$\langle b\beta'\rvert$	$\tau\sin(\theta/2)$	$\tau\cos(\theta/2)$	0	KS_B

(6.31)

In the case of $S_A = S_B = S$, the diagonalization of the matrix leads to four eigenvalues which read as follows:

$$E = \frac{1}{2}K \pm \sqrt{\big(K(S+{}^1\!/_2) \pm \tau\cos(\theta/2)\big)^2 + \tau^2\sin^2(\theta/2)} \tag{6.32}$$

Figure 6.6 gives a clue on how to simplify this expression. In the first place, we see that $\cos(\theta/2)$ can be written as $S_0/2S$ with $S_0 = |\mathbf{S}_A + \mathbf{S}_B|$. In a classical description, that is in the limit of infinitely large S_0, the alignment of the spin moment of the extra electron to S_0 is irrelevant and the total spin moment of the system S_T is

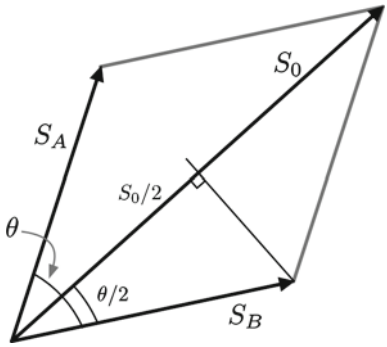

Fig. 6.6 Definition of S_0 as $|\mathbf{S}_A + \mathbf{S}_B|$ and $\cos(\theta/2)$ as $S_0/2S$

directly equal to S_0. Applying the same correction for the quantum nature of the spin moments as done in Eq. 6.30, we obtain $\cos(\theta/2) = (S_0 + 1/2)(2S_{max} + 1)$, where $S_{max} = |\mathbf{S}_A + \mathbf{S}_B| + \frac{1}{2}$, corresponding to the maximum spin moment that can be realized by all the unpaired electrons. The second simplification arises from the fact that $\tau \ll K$ and justifies the neglect of the term quadratic in τ in the square root. The expression for the energy now becomes

$$E = \frac{1}{2}K \pm \left(K(S+{}^1\!/_2) \pm \tau\cos(\theta/2)\right) = \frac{1}{2}K \pm \left(KS + \frac{1}{2}K\right) \pm \tau\frac{S_0 + 1/2}{2S_{max}+1} \quad (6.33)$$

By choosing the reference energy equal to $-KS$, the expression reduces to

$$E_- = \pm\tau\frac{S_0 + 1/2}{2S_{max}+1} \quad (6.34)$$

$$E_+ = K + 2KS \pm \tau\frac{S_0 + 1/2}{2S_{max}+1} \quad (6.35)$$

Considering the quantum correction due to the use of spin eigenfunctions, τ can be replaced by $2t$, which turns the expression for E_- into the first term of Eq. 6.26 and describes the energies of the low-lying states with the spin moment of the extra electron parallel aligned with $\mathbf{S}_A$ or $\mathbf{S}_B$. E_+ applies to the states with anti-parallel alignment, and hence, lie at much higher energy.

6.3 A Quantum Chemical Approach to Magnetic Interactions in the Solid State

Many of the macroscopic manifestations of the interaction between localized, delocalized or itinerant unpaired electrons in solid state compounds require a description that goes far beyond the possibilities of the computational schemes that are routinely applied in molecular quantum chemistry. The theoretical treatment of the

long-range magnetic ordering, Kondo effect, domain formation, superconductivity, metal-insulator transitions, etc. belongs typically to the field of condensed matter physics and several excellent books have been published on this topic, see for example Refs. [7–10]. This does however not mean that quantum chemistry cannot contribute to the understanding of magnetic phenomena in solid state compounds. We have already seen in Sect. 3.3 how the calculation of the magnetic interaction parameters can serve as the basis for the calculation of the magnetic susceptibility and the determination of the magnetic structure, or more precise the magnetic unit cell. In fact, a large part of the parameters that typically appear in the model Hamiltonians of condensed matter physics can be calculated accurately through quantum chemical calculations provided that one can establish an accurate finite representation of the relevant part of the crystal. In the case of molecular crystals, this issue is nearly trivially answered: taking one or several discrete units as model often suffices to calculate the desired microscopic electronic structure parameters. The situation becomes more complicated when dealing with ionic lattices (oxides, pnictides among others) and is even worse for crystals with only covalently bonded atoms (e.g. silicon or graphene doped with holes). There are however several well-established approaches to extract reliable information at least for the ionic crystals. Also in the more difficult case of (partly) covalent lattices quantum chemical strategies can offer interesting insights in the electronic structure related to magnetic interactions.

6.3.1 Embedded Cluster Approach

The intrinsic local nature of the interaction between two localized spin moments suggests the possibility to study the magnetic interactions in solids with a cluster model. In this approach, a small yet relevant piece is cut from the crystal and treated like a molecule. These bare clusters are only a reasonable choice in the case of molecular crystals, but otherwise nearly always too crude a representation. Therefore it is necessary to account for the effect of the rest of the crystal especially when dealing with ionic or covalent lattices. Here, we will shortly review a few representative examples of the different approaches for improving the bare cluster model that find their basis in the theory of electron separability of McWeeny, the subsystem formulation of DFT of Cartona or the incremental scheme of Fulde and Stoll.

Electrostatic embedding: In the case of ionic compounds, the largest contribution to the potential exerted by the rest of the crystal on the (central region of the) cluster is due to long-range electrostatic interactions. These are accurately represented by the point charge approximation, that is, the Madelung potential:

$$V_M(\kappa \in \mathbb{K}) = \sum_{\lambda \in \mathbb{L}} \frac{q_\kappa q_\lambda}{r_{\kappa\lambda}} \tag{6.36}$$

where $\mathbb{K}$ is the set of ions that belong to the cluster and $\mathbb{L}$ contains all other ions, q corresponds to the formal ionic charge of each center. This interaction is easily included in the calculation by placing an array of point charges around the cluster at the lattice sites. Their value is either taken as the formal ionic charge (with fractional charges on the edge of the array to ensure charge neutrality) or fitted in such a way that a relatively small set of point charges reproduces the electrostatic effect of the whole crystal.

The presence of point charges at lattice sites in the immediate neighbourhood of the cluster often artificially polarizes the electron density of the cluster. This polarization is especially large when the cluster has anions on the outside and the first shell of charges contains positive charges. Actually, this is the common situation when magnetic interactions in ionic transition metal compounds are studied. The usual cluster has two (or sometimes more) transition metals and the anions (O^{2-}, F^{-}, etc.) of the first coordination sphere. The first shell around this cluster is formed by either the transition metal ions, ternary cations or a combination of these, depending on the crystal structure. In any case, positive point charges are located directly around the highly polarizable anions causing important distortions of the electronic structure not only in the border regions of the cluster, but also in the central part. To improve the description a border region is created between the point charges and the cluster. In this intermediate region the lattice sites are occupied by potentials that model the Coulomb and exchange interactions between the electron density of the cluster and the ions in the intermediate region [11]. Figure 6.7 shows how the potentials separate the cluster from the bare point charges and avoid the artificial polarization of the cluster electron density.

Density-based embeddings: This approach starts with a calculation on the whole system to construct an approximate yet accurate representation of the total density ρ_{tot} by performing a periodic DFT calculation. Then, a guess density of the cluster is constructed from a calculation on the isolated unit or using some simple embedding scheme as described above. The total density is now divided in two parts $\rho_{tot} = \rho_1 + \rho_2$ and the one-electron embedding potential is constructed from the functional derivative of interaction energy with respect to the cluster density ρ_1.

$$\begin{aligned} E^{int} &= T_s^{int} + E_{ne}^{int} + E_{xc}^{int} + E_H^{int} + E_{nn}^{int} \\ v_{emb}(r) &= \frac{\partial E_{int}}{\partial \rho_1} \end{aligned} \tag{6.37}$$

where the interaction energy is written as a sum of the kinetic, electron-nuclear, exchange correlation, Coulomb repulsion, and nuclear repulsion energy. This embedding potential is added to the standard Kohn-Sham equation for the cluster and a new energy and density ρ_1 are calculated. Since the embedding potential depends on the density of the cluster, v_{emb} is updated and the Kohn-Sham equations of the cluster are solved again. This process is repeated until a self-consistent description is obtained. In addition to the here sketched DFT in DFT (cluster in embedding) procedure, the variants with wave function (WF) based methods have also been described. The

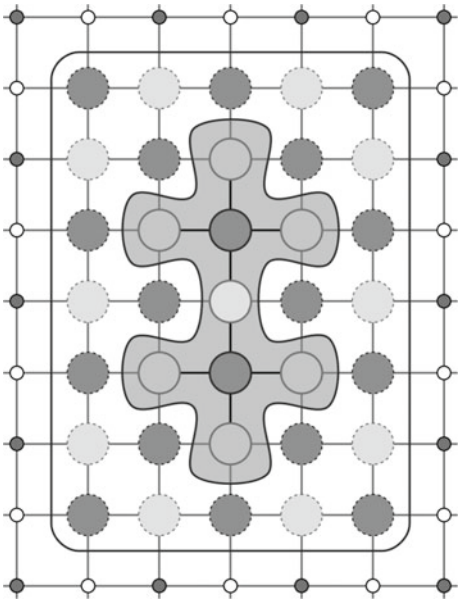

Fig. 6.7 Two-dimensional impression of a typical embedded cluster model to calculate the interaction strength between two spin moments. The atoms in the *shaded area* constitute the cluster, the *small spheres* on the outside constitute the first shell of positive and negative bare point charges (the rest is not shown), and the spheres with the *dotted outline* in the intermediate region are model potentials that separate the cluster from the point charges

WF in DFT approach is especially interesting for the application to systems with unpaired electrons because the multideterminental nature of the wave function can be rigorously treated while the embedding can be generated with DFT.

Induced dipoles: There are also embedding schemes that go beyond the static representation of the cluster environment and model the polarization of the electron density in response to changes in the electronic structure of the cluster, for example ionizations or electron excitation processes. In the so-called shell model, the bare point charges are split in a positive point charge (the nucleus) and a negative shell (the electron cloud of the ion) connected through a harmonic potential. The shells interact with a Buckingham potential and the total energy of the system (cluster + shell environment) is minimized not only with respect to the electron distribution in the cluster region but also with respect to the position of the shells. Another scheme places a set of polarizable dipoles in the environment and the values of the induced dipoles are optimized in a self-consistent procedure along with the electron density of the cluster.

Once, a convenient embedded cluster model is constructed, one can apply all the regular methods from molecular quantum chemistry to evaluate the electronic structure parameters of interest, hopping parameters, magnetic coupling strength, local anisotropy, biquadratic exchange, etc. The validity of the embedded cluster model has been established in many applications either by comparing the results to periodic calculations or by checking the stability of the results against the size of the cluster.

6.3.2 Periodic Calculations

Magnetic interactions in extended systems can also be studied without creating the more or less approximate representation of the material with an embedded cluster. The approach based on the translational symmetry in the crystal naturally leads to the well-known band structures of the Bloch functions, periodic one-electron functions.

$$\psi_k(r) = \sum_{r'} e^{i\mathbf{k}\cdot\mathbf{r}'} \phi(r') \tag{6.38}$$

The difficulty of constructing spin eigenfunctions with $S < S_{max}$ for extended systems with unpaired electrons makes that most of the periodic calculations are performed within a single determinant method and no restrictions on the spatial part of the spin orbitals. The results are then necessarily interpreted with the Ising model Hamiltonian described in Sect. 3.2.2. In practice, the total energy of the magnetic unit cell (not necessarily of the same size as the structural unit cell) is calculated for different spin orientations (that is, different M_S values) and the relative energies are compared to the matrix elements of the Ising Hamiltonian to determine the magnetic coupling strength between the ions in the crystal. This is not necessarily limited to isotropic bilinear coupling but can also be used to extract estimates for biquadratic and four-center interactions.

To illustrate the procedure of extracting magnetic coupling parameters by periodic calculations, we will focus on the perovskite structure Sr_2CuO_3, related to the previously used spin ladder compound $SrCu_2O_3$, although the structural motif here is formed by CuO_4 units arranged in linear chains along the b-axis of the unit cell. Figure 6.8 illustrates the structure of this oxide and indicates the unit cell with a dashed box. The unit cell has two symmetry inequivalent Cu^{2+} ions with an $S = \frac{1}{2}$ spin moment each.

In the first place, we calculate the energy per unit cell with all spins aligned ferromagnetically as schematically depicted in the left panel of Fig. 6.9. This calculation can be done within any spin unrestricted periodic computationally scheme, either HF or DFT and it gives us $E_F(a, b, c)$. Subsequently, this energy has to be expressed as an Ising energy. The Ising Hamiltonian for this compound is defined as

$$\hat{H} = -J_a \sum_{i,j} \hat{S}_{z,i}\hat{S}_{z,j} - J_b \sum_{k,l} \hat{S}_{z,k}\hat{S}_{z,l} - J_d \sum_{m,n} \hat{S}_{z,m}\hat{S}_{z,n} \tag{6.39}$$

where the interaction along the c-direction is neglected and J_d is the interaction along the body diagonal of the unit cell. As can be seen in the left panel of Fig. 6.9, the unit cell contains 8 times the interaction along the body diagonal. The four vertices along a and b represent the J_a and J_b interactions, but each of these have to be counted only for 1/4 since the vertices are shared by four unit cells. Furthermore, the copper ion in the center of the unit cell interact with the copper ions in the adjacent unit cells and this contributes two times $1/2J_a$ and two times $1/2J_b$ to the Ising energy. In total the energy expression becomes

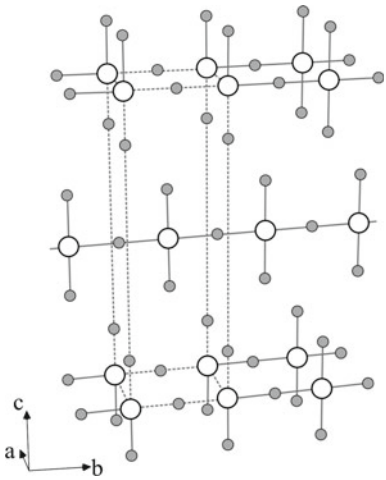

Fig. 6.8 Graphical representation of the perovskite Sr_2CuO_3. The unit cell is given as a *dashed box*. Cu ions are represented as *large white spheres* and oxygen as *smaller gray spheres*, Sr ions are not depicted for clarity

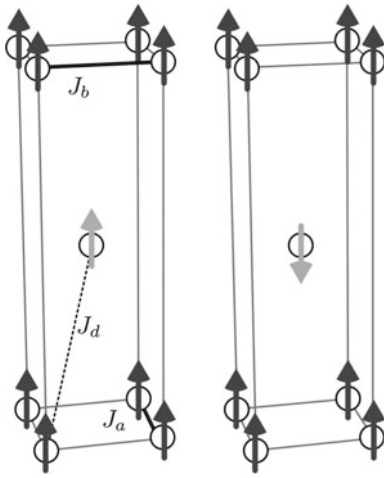

Fig. 6.9 Ferromagnetic (*left*) and antiferromagnetic (*right*) spin settings in the unit cell of Sr_2CuO_3. The spin on symmetry equivalent copper ions are marked with the same *gray scale*

$$E_F(a,b,c) = -J_a\left(4\cdot\frac{1}{2}\cdot\frac{1}{2}/4 + 2\cdot\frac{1}{2}\cdot\frac{1}{2}/2\right) - J_b\left(4\cdot\frac{1}{2}\cdot\frac{1}{2}/4 + 2\cdot\frac{1}{2}\cdot\frac{1}{2}/2\right)$$
$$- J_d\cdot 8\cdot\frac{1}{2}\cdot\frac{1}{2} = -2J_d - \frac{1}{2}J_a - \frac{1}{2}J_b \tag{6.40}$$

The second step consists of the calculation of the energy per unit cell after flipping the spin on the central copper (right panel of Fig. 6.9) and relating it to the energy expression obtained with the Ising Hamiltonian. As far as the interactions along a and b are concerned, the situation remains unchanged with respect to the ferromagnetic alignment. The expression only changes for the interaction along the

diagonal, since $\hat{S}_{z,m}$ and $\hat{S}_{z,n}$ result now in $\frac{1}{2}$ and $-\frac{1}{2}$. With this, the expression is readily written down as

$$E_{AF}(a,b,c) = 2J_d - \frac{1}{2}J_a - \frac{1}{2}J_b \tag{6.41}$$

and from the energy difference of the two calculations, we can determine J_d

$$E_{AF}(a,b,c) - E_F(a,b,c) = 4J_d \tag{6.42}$$

The calculation of J_b (and J_a) cannot be done with the simple unit cell, no other spin flips can be made. Therefore, we double the unit cell in the b direction to obtain a new *magnetic* unit cell, the super cell $(a, 2b, c)$, represented in Fig. 6.10. The energy of the fully ferromagnetic supercell is in principle exactly twice $E_F(a,b,c)$, but it is highly recommendable to repeat the HF or DFT calculation for this double unit cell due to numerical precision issues. Subsequently, we flip the spins on the copper ions in the middle of the cell to obtain a spin arrangement with antiferromagnetic ordering along the b-axis. A careful analysis of the interactions contained in these two magnetic unit cells gives the energy expressions of the Ising Hamiltonian

$$E_F(a,2b,c) = 2E_F(a,b,c) = -4J_d - J_a - J_b \tag{6.43}$$

$$E_{AF}(a,2b,c) = -J_a + J_b \tag{6.44}$$

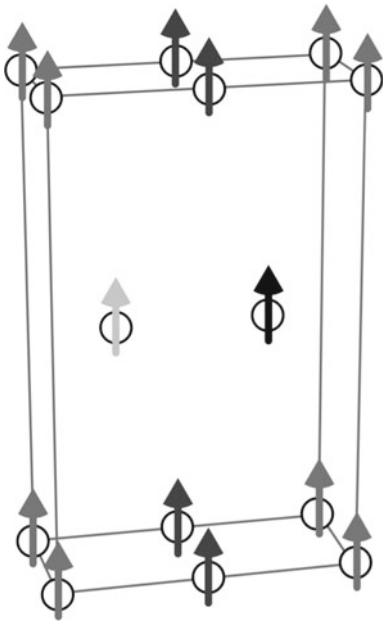

Fig. 6.10 Magnetic unit cell obtained by doubling the simple unit cell along the b direction. Symmetry equivalent copper ions have spins with the same *gray scale*. The antiferromagnetic unit cell is obtained by flipping the *dark gray* spins at the lattice positions (0,1,0) and $(\frac{1}{2}, \frac{3}{2}, \frac{1}{2})$

and the energy difference of the two spin arrangements becomes

$$E_{AF}(a, 2b, c) - E_F(a, 2b, c) = 4J_d + 2J_b \tag{6.45}$$

which allows us to extract J_b, given that J_d is already determined in the simple unit cell calculations. To calculate J_a one should double the unit cell along the a direction and follow the same strategy as for the $(a, 2b, c)$ super cell.

Method of increments: By taking the appropriate linear combinations of the delocalized Bloch functions one can construct orbitals that are localized on an atom or a small group of atoms of the crystal. These so called Wannier orbitals form the basis of the method of increments for calculating the cohesive energy of an extended solid [12, 13] and other related properties such as lattice constants, bulk modulus, absorption energies, among others. Excited state properties can also be studied and from there one has access to the band structure. The method was originally formulated for closed shell systems, but recently variants have been developed to treat compounds with unpaired electrons. Hence, the method can in principle also be used for the study of magnetic interactions in solids.

In its most basic formulation, the procedure starts with a periodic Hartree-Fock calculation. The correlation energy is calculated by *increments*. The unit cell is divided in m subunits A_i, either individual atoms or small clusters of atoms. The Bloch functions optimized in the periodic HF calculation are transformed to Wannier functions that are localized on the different subunits and the local correlation energy $E_i^{corr} = E_i^{tot} - E_i^{HF}$ is calculated for each subunit A_i with a standard (size-extensive) post-HF method. This is not the final estimate because all non-additive terms in the correlation energy are still missing. Therefore one subsequently calculates the two-center corrections through calculations on subunits A_i–A_j: $E_{ij}^{corr} = E_{ij}^{tot} - E_{ij}^{HF} - E_i^{corr} - E_j^{corr}$. The index i runs over all groups in the unit cell, but j can in principle be any atom (group of atoms) in the system. Fortunately, the size of the increment decays rapidly with the distance between the groups and hence the number of terms to be calculated remains relatively small. This can be repeated with three-center corrections and higher order increments. The total correlation energy is then determined

$$E^{corr} = \sum_i E_i^{corr} + \frac{1}{2}\sum_{i\neq j} E_{ij}^{corr} + \frac{1}{6}\sum_{i\neq j\neq k} E_{ijk}^{corr} + \ldots \tag{6.46}$$

and added to the Hartree-Fock energy of the periodic calculation.

Correlated band structures: Periodic single determinant approaches are well suited to give qualitative answers or to serve as benchmark for checking the validity of embedded cluster results. On the other hand, the accurate treatment of (strong) electron correlation effects in crystalline materials, for example to predict the subtle interplay of magnetism and electrical conductance, requires an accurate, balanced description of all states involved, and this is still a challenge.

Examples of strongly correlated systems are transition metal and rare-earth metal compounds. In these materials on-site Coulomb repulsion between the metal valence electrons dominates the width of the corresponding one-electron energy bands. Widely used independent electron methods such as DFT in the local density approximation (LDA) are not suited to study the magnetic properties of such systems. Therefore, a correction term U to the LD functional has been introduced that accounts for the strong on-site Coulomb interactions between d (or f) electrons on the metal ions, giving rise to the LDA+U method [14]. Although LDA+U was introduced as a method without adjustable parameters, the values used for U vary significantly in different studies on the same compound.

Within Green function theory, many-electron effects can be introduced through a non-local and energy-dependent self-energy operator [15]. Since the self-energy is hard to calculate, various approximations are introduced and among the simplest ones is the so-called GW approximation, which is derived from many-body perturbation theory. Although the GW approximation offers in principle a sophisticated account of the electron correlation effects, practical realizations are commonly also based on the LDA method.

Finally, algorithms have been developed which incorporate electron correlation effects explicitly in wave function based band theory for crystalline solids [16, 17]. These algorithms construct the many-electron Hamiltonian matrix for a periodic system by extracting the matrix elements from calculations on finite embedded clusters. In this way the incorporation of correlation effects leads to many-electron energy bands, not only associated with hole states and added-electron states but also with excited states. More recently, Pisani and co-workers [18] introduced a post-Hartree-Fock program based on periodic local second order Møller-Plesset perturbation theory.

A word of warning is in place when these techniques are employed for the study of magnetic interactions. The tiny energy differences associated with these interactions demand that the procedure is capable to deliver not only an accurate but also a balanced treatment of the various states involved. This means that approximate computation and cut-offs of integrals etc. have to be exactly the same for all states.

6.4 Goodenough–Kanamori Rules

The Goodenough–Kanamori (GK) rules have evolved from the studies to explain the magnetism in manganese oxides in the 1950s and have been applied ever since mostly in the field of ionic insulators; often oxides of one or several third-row transition metal ions. Studies of the magnetic interactions in these compounds commonly reduce to a three center problem with two metals that carry a spin moment and a non-magnetic anion in between. Before explaining the rules, which are sometimes (incorrectly) referred to as the Goodenough–Kanamori–Anderson rules, we need to introduce some concepts related with the electron hopping involving the magnetic sites and the ligand that connects them. Goodenough defined *superexchange* as the virtual electron

transfer between two atoms with a net spin moment and *semi covalent exchange* as the virtual electron transfer between the anion and the two magnetic centers. Note that Goodenough's definition of superexchange differs from the one given by Kramers (see Sect. 3.1).

To understand the use of the term *virtual* in these definitions it is best to contrast it against the electron hopping discussed in the previous section for doped or mixed-valence systems. These processes represent a real electron movement in which the formal oxidation state of the metals changes by ± 1. There are three different cases as defined in Eq. 6.1, which correspond to electron movement from half-filled to an empty orbitals, from half-filled to half-filled and from filled to half-filled orbitals. On the contrary a virtual electron transfer process does not cause changes in oxidation state and the initial electron count per atom is always restored. It can very much be compared to the perturbative interaction paths introduced in Chap. 5, the super-exchange is comparable to the mechanism shown in Fig. 5.3 and the semi covalent exchange is strongly related to the one depicted in Fig. 5.4. The direct exchange K_{ab} is normally not considered in the GK reasonings to explain magnetic interactions in solid state compounds.

The Goodenough–Kanamori rules state that superexchange and semi covalent exchange give an antiferromagnetic contribution to the coupling of the spin moments on site A and B when the virtual electron transfer is between overlapping orbitals that are half-filled. A ferromagnetic contribution arises when the virtual transfer is from half-filled to empty orbitals or from filled to half-filled orbitals. Moreover it is taken for granted that the electron transfer can only take place between overlapping orbitals. For orthogonal orbitals, the hopping is zero and Hund's rule prevails leading to a ferromagnetic contribution (Fig. 6.11).

Figure 6.12 illustrates the prototypical case of the magnetic interactions in the CuO_2 layers of the parent compounds of the high T_c superconductors. The Cu^{2+} ions have a $3d^9$ electronic configuration with one unpaired electron in the $3d_{x^2-y^2}$ orbital.

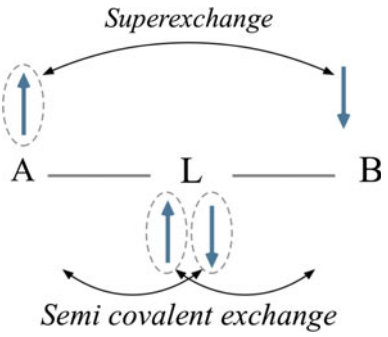

Fig. 6.11 Representation of the two *virtual* electron exchange mechanisms that are the basis of the Goodenough–Kanamori rules. *Above* the virtual exchange between two atoms (A and B) with non-zero spin moment, known as *superexchange* and *below* the virtual exchange between two atoms and a shared anion, the so-called *semi covalent exchange*

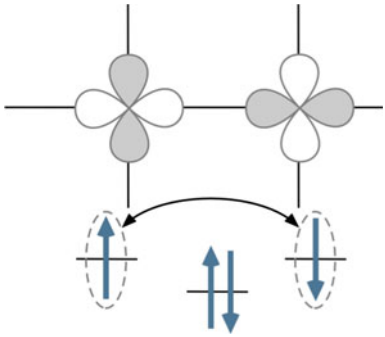

Fig. 6.12 Virtual electron superexchange between two overlapping half-filled orbitals leading to antiferromagnetic coupling

The virtual electron transfer between these two copper atoms, i.e. the superexchange, involves half-filled orbitals and hence contributes in an antiferromagnetic manner to the coupling. The semi covalent exchange contributes in the same direction, since it also involves the half-filled orbitals on the metals. Together the two effects give a qualitative explanation of the strong antiferromagnetic interactions between the Cu^{2+} ions.

The second example concerns $LaMnO_3$, which upon hole-doping shows a spectacular drop in the electrical resistivity when an external magnetic field is applied, the so-called colossal magnetoresistance effect. The electronic configuration of the Mn^{3+} ions is $3d^4$, with three unpaired electrons in the t_{2g} and one in the e_g orbitals assuming an octahedral coordination of the Mn cations. However, this configuration is Jahn-Teller active and induces displacements of the oxygen anions as indicated by the arrows in the left part of Fig. 6.13. In consequence, the occupied $3d$-orbitals of e_g symmetry are rotated by 90° at each magnetic center. This is called *orbital ordering* in the literature. Now, the superexchange between half-filled e_g orbitals cannot take place because they are orthogonal as shown in the left panel of Fig. 6.13. The only overlapping e_g orbitals are the half-filled on the left and the empty orbital on the right, see the right side of Fig. 6.13. The GK rules state that this superexchange (and the semi covalent exchange as well) is ferromagnetic in nature. The total interaction between the two magnetic centers is therefore expected to be ferromagnetic, although attenuated by the superexchange interactions in the weakly overlapping half-filled $3d(t_{2g})$ orbitals.

In previous chapters we have considered the magnetic interactions in the spin ladder compound $SrCu_2O_3$. There we focused on the interactions along the legs and the rungs, which share the common feature of a linear Cu–O–Cu linkage. However, taking a closer look at the structure (see Fig. 5.9) it becomes immediately clear that these copper ions are not nearest neighbours. Instead, the distance to the copper ion on the next ladder is shorter and one could naively think that the interactions of such pairs are also important. We have already seen in Sect. 4.2 that the interaction between two magnetic centers connected by a (double) bridge making an angle of around 90° is in general ferromagnetic and rather weak. A qualitative picture of the weak ferromagnetic interaction can also be obtained by applying the GK rules. The

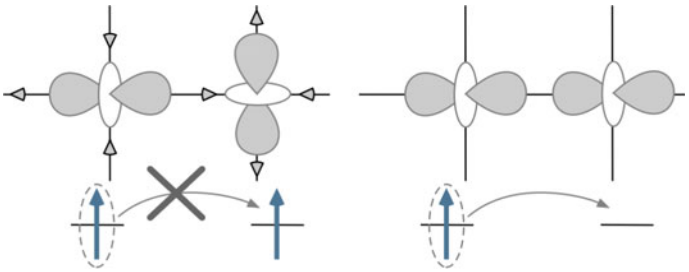

Fig. 6.13 The virtual hopping on the *left* is not permitted due to the orthogonality of the (occupied) orbitals on the two centers. The superexchange on the *right* is due to a virtual electron hopping from a half-filled to an empty orbital and hence ferromagnetic in character

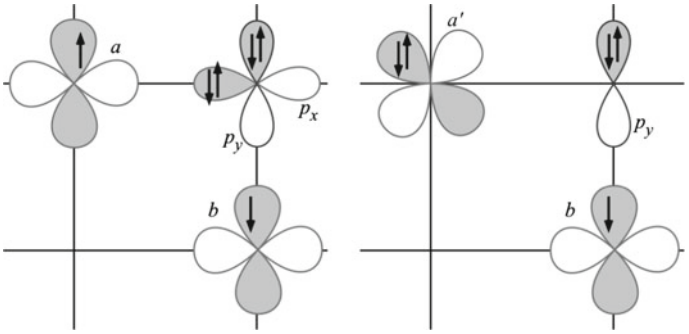

Fig. 6.14 *Left* the superexchange between a and b gives a small antiferromagnetic contribution. The semi covalent exchange with a and b is inoperative. *Right* Ferromagnetic contribution to the coupling by semi covalent exchange with a half-filled and a filled orbital

half-filled orbitals a and b shown on the left side of Fig. 6.14 overlap, and hence, the superexchange mechanism gives a antiferromagnetic contribution, albeit rather small since the overlap is not very strong. The semi covalent exchange involving a and b is inoperative because these two half-filled orbitals do not overlap with the same orbital on the anion. To activate the semi covalent exchange we have to consider one of the filled $3d$ orbitals that overlaps with one of the ligand orbitals, which in turn has a non-zero overlap with the half-filled $3d$ orbital on the other cation. Such situation is outlined in the right panel of Fig. 6.14, where a' is one of the doubly occupied $3d(t_{2g})$ orbitals (to be more precise the $3d_{xy}$ in this case) and b the half-filled $3d_{x^2-y^2}$ orbital. Whereas the overlap of a' and b is zero (no superexchange) both orbitals overlap with the O-$2p_y$ orbital and the semi covalent exchange becomes active. Since the virtual electron transfer is between a filled and a half-filled orbital, the contribution is ferromagnetic.

A pictorial explanation for the ferromagnetic nature of the semicovalent exchange between filled and half-filled orbitals is given in Fig. 6.15. In the upper part, we can see how the subsequent electron transfer from p_y to b and from a' to p_y leads to a

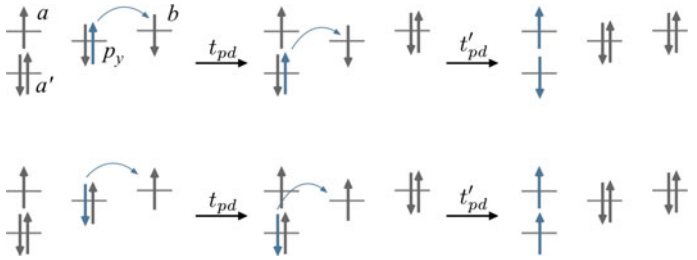

Fig. 6.15 Semi covalent exchange between filled and half-filled orbitals as operative in the magnetic coupling between two copper ions with an oxygen bridge forming an angle of 90°. *Upper part* for antiferromagnetic coupling, and *below* for ferromagnetic interaction

non-Hund determinant with two anti-parallel electrons on center A. This unfavorable electronic configuration is avoided in the case of a ferromagnetically coupled initial state shown in the lower part of the figure.

Estimation with perturbation theory: The ferromagnetic nature of the interaction between two magnetic centers with $S = \frac{1}{2}$ through a ligand under an angle of 90° can also be rationalized with perturbation theory in the same way as discussed in Sect. 5.1.1 for the magnetic interactions in a linear geometry or in Sect. 5.4.3 to derive the equations to estimate the magnitude of the four-center interactions with single determinant methods. The derivation is similar to the one presented by Koch in Ref. [19] with this difference that we here work within a spin restricted formalism.

There are four orbitals involved in the coupling as can be seen in Fig. 6.14. The six electrons can be distributed in sixteen different ways over the orbitals under the restriction of $M_S = 0$:

$$\Phi_1 = |a_1 p_x \bar{p}_x p_y \bar{p}_y \bar{b}_2| \quad \Phi_2 = |\bar{a}_1 p_x \bar{p}_x p_y \bar{p}_y b_2| \quad \Phi_3 = |a_1 \bar{p}_x p_y \bar{p}_y b_2 \bar{b}_2|$$
$$\Phi_4 = |\bar{a}_1 p_x p_y \bar{p}_y b_2 \bar{b}_2| \quad \Phi_5 = |a_1 \bar{a}_1 p_x \bar{p}_x p_y \bar{b}_2| \quad \Phi_6 = |a_1 \bar{a}_1 p_x \bar{p}_x \bar{p}_y b_2|$$
$$\Phi_7 = |a_1 \bar{a}_1 p_x p_y \bar{p}_y \bar{b}_2| \quad \Phi_8 = |a_1 \bar{a}_1 \bar{p}_x p_y \bar{p}_y b_1| \quad \Phi_9 = |a_1 p_x \bar{p}_x \bar{p}_y b_2 \bar{b}_2|$$
$$\Phi_{10} = |\bar{a}_1 p_x \bar{p}_x p_y b_2 \bar{b}_2| \quad \Phi_{11} = |a_1 \bar{a}_1 p_x \bar{p}_y b_2 \bar{b}_2| \quad \Phi_{12} = |a_1 \bar{a}_1 \bar{p}_x p_y b_2 \bar{b}_2|$$
$$\Phi_{13} = |a_1 \bar{a}_1 p_x \bar{p}_x p_y \bar{p}_y| \quad \Phi_{14} = |p_x \bar{p}_x p_y \bar{p}_y b_2 \bar{b}_2| \quad \Phi_{15} = |a_1 \bar{a}_1 p_x \bar{p}_x b_2 \bar{b}_2|$$
$$\Phi_{16} = |a_1 \bar{a}_1 p_y \bar{p}_y b_2 \bar{b}_2|$$

Taking the energy of Φ_1 and Φ_2 as reference, the other determinants lie at ΔE_{CT} ($\Phi_3 \ldots \Phi_6$), $\Delta E'_{CT}$ ($\Phi_7 \ldots \Phi_{10}$), ΔE_{2CT} (Φ_{11} and Φ_{12}), U_d (Φ_{13} and Φ_{14}) and $\Delta E_{2CT} + U_p$ (Φ_{15} and Φ_{16}). The last two determinants are high in energy and will be neglected. The subscript p refers to the O-2p_x or 2p_y orbital and the subscript d to the a or b Cu-3d orbital.

To simplify the derivation of the singlet and triplet energy, we first construct spin-symmetry adapted CSFs by forming linear combination of the above-listed determinants with unpaired electrons:

$$\Psi_{1,2} = \frac{1}{\sqrt{2}}(\Phi_1 \pm \Phi_2) \qquad \Psi_{3,4} = \frac{1}{\sqrt{2}}(\Phi_1 \pm \Phi_2) \qquad \Psi_{5,6} = \frac{1}{\sqrt{2}}(\Phi_5 \pm \Phi_6)$$
$$\Psi_{7,8} = \frac{1}{\sqrt{2}}(\Phi_7 \pm \Phi_8) \qquad \Psi_{9,10} = \frac{1}{\sqrt{2}}(\Phi_9 \pm \Phi_{10}) \qquad \Psi_{11,12} = \frac{1}{\sqrt{2}}(\Phi_{11} \pm \Phi_{12})$$
$$\Psi_{13,14} = \frac{1}{\sqrt{2}}(\Phi_{13} \pm \Phi_{14})$$

The plus (minus) combinations are triplet (singlet) functions, except for the combination of closed-shell determinants Ψ_{13} and Ψ_{14}, which are both singlets. Now we can construct the 6×6 configuration interaction matrix for the triplet functions and an 8×8 matrix for the singlet and then determine the energy either by diagonalizing the matrices or (simpler) with perturbation theory.

$S = 1$	$\|\Psi_1\rangle$	$\|\Psi_3\rangle$	$\|\Psi_5\rangle$	$\|\Psi_7\rangle$	$\|\Psi_9\rangle$	$\|\Psi_{11}\rangle$
$\langle\Psi_1\|$	0	0	0	$-t_{pd}$	$-t_{pd}$	0
$\langle\Psi_3\|$	0	ΔE_{CT}	0	t_{ab}	0	0
$\langle\Psi_5\|$	0	0	ΔE_{CT}	0	t_{ab}	0
$\langle\Psi_7\|$	$-t_{pd}$	t_{ab}	0	$\Delta E'_{CT}$	0	$-t_{pd}$
$\langle\Psi_9\|$	$-t_{pd}$	0	t_{ab}	0	$\Delta E'_{CT}$	$-t_{pd}$
$\langle\Psi_{11}\|$	0	0	0	$-t_{pd}$	$-t_{pd}$	$\Delta E_{2CT} - K_{xy}$

$S = 0$	$\|\Psi_2\rangle$	$\|\Psi_4\rangle$	$\|\Psi_6\rangle$	$\|\Psi_8\rangle$	$\|\Psi_{10}\rangle$	$\|\Psi_{12}\rangle$	$\|\Psi_{13}\rangle$	$\|\Psi_{14}\rangle$
$\langle\Psi_2\|$	0	0	0	$-t_{pd}$	$-t_{pd}$	0	$2t_{ab}$	0
$\langle\Psi_4\|$	0	ΔE_{CT}	0	$-t_{ab}$	0	0	t_{pd}	$-t_{pd}$
$\langle\Psi_6\|$	0	0	ΔE_{CT}	0	$-t_{ab}$	0	t_{pd}	t_{pd}
$\langle\Psi_8\|$	$-t_{pd}$	$-t_{ab}$	0	$\Delta E'_{CT}$	0	$-t_{pd}$	0	0
$\langle\Psi_{10}\|$	$-t_{pd}$	0	$-t_{ab}$	0	$\Delta E'_{CT}$	$-t_{pd}$	0	0
$\langle\Psi_{12}\|$	0	0	0	$-t_{pd}$	$-t_{pd}$	$\Delta E_{2CT} + K_{xy}$	0	0
$\langle\Psi_{13}\|$	$2t_{ab}$	t_{pd}	t_{pd}	0	0	0	U_d	0
$\langle\Psi_{14}\|$	0	$-t_{pd}$	t_{pd}	0	0	0	0	U_d

In these matrices we have neglected the intersite exchange integrals K_{ab} and K_{pd}. The hopping parameter t_{ab} parametrizes the electron transfer from cation to cation and t_{pd} the transfer from O-$2p_x$ to a and from p_y to b, which are strictly the same. The hopping from p_y to a is zero by symmetry. This is most easily seen in Fig. 6.14 (left). The symmetry behavior under 180° rotation around the x-axis is different for p_y (changes sign) and for a (no sign change). Because the Hamiltonian is totally symmetric, the integral $\langle p_y|\hat{h}|a\rangle$ is zero. A similar reasoning shows that the hopping from p_x to b is zero.

In an order-by-order perturbational approach we will derive the singlet-triplet energy gap to estimate the character and size of the magnetic coupling of the two Cu^{2+} ions bridged by an oxygen anion under 90°. Up to first order, the energies are zero for the lowest singlet and triplet functions: $\langle\Psi_1|\hat{H}|\Psi_1\rangle = \langle\Psi_2|\hat{H}|\Psi_2\rangle = 0$. Remember that the intersite exchange interactions have been neglected, otherwise the zeroth-order triplet-singlet gap would be $2K_{ab}$. The second-order correction to the energy of the triplet and singlet are

$$\text{Triplet: } E_T^{(2)} = \frac{|\langle\Psi_1|\hat{H}|\Psi_7\rangle|^2}{E_0 - E_7} + \frac{|\langle\Psi_1|\hat{H}|\Psi_9\rangle|^2}{E_0 - E_9} = \frac{-2t_{pd}^2}{\Delta E'_{CT}} \tag{6.47a}$$

$$\text{Singlet: } E_S^{(2)} = \frac{-2t_{pd}^2}{\Delta E'_{CT}} - \frac{4t_{ab}^2}{U_d} \tag{6.47b}$$

The singlet is lower in energy by $4t_{ab}^2/U_d$, which corresponds to the antiferromagnetic superexchange by the direct electron transfer between the half-filled orbitals. The energy lowering is however small since t_{ab} is in general very small as long as there is no delocalization onto the ligand, conform the discussion of the valence mechanisms in Sect. 5.1.1. Note that the electron transfer from ligand to metal does give a significant energy lowering but that the differential effect is zero, the contribution to both states is the same.

6.5 Demonstrate that the energies up to second-order are given by the expressions in Eq. 6.47.

At fourth-order perturbation, there are many more contributions, but a large part is again identical for singlet and triplet. Only the contributions that involve Ψ_{11}, Ψ_{12} and Ψ_{13} have a differential effect. These can be separated in two contributions. First, the singlet-only contribution involving Ψ_{13} and second with either Ψ_{11} (singlet) or Ψ_{12} (triplet). The singlet-only contribution is given by

$$\sum_{i=4,6} \frac{\langle\Psi_2|\hat{H}|\Psi_{13}\rangle\langle\Psi_{13}|\hat{H}|\Psi_i\rangle\langle\Psi_i|\hat{H}|\Psi_{13}\rangle\langle\Psi_{13}|\hat{H}|\Psi_2\rangle}{-E_i \cdot E_{13}^2} = -\frac{8t_{ab}^2 t_{pd}^2}{\Delta E_{CT} U_d^2} \tag{6.48}$$

The fourth-order differential contribution to the triplet is

$$\sum_{i,j=7,9} \frac{\langle\Psi_1|\hat{H}|\Psi_i\rangle\langle\Psi_i|\hat{H}|\Psi_{11}\rangle\langle\Psi_{11}|\hat{H}|\Psi_j\rangle\langle\Psi_j|\hat{H}|\Psi_1\rangle}{-E_i \cdot E_j \cdot E_{11}}$$

$$= -\frac{16t_{pd}^4}{(\Delta E'_{CT})^2(\Delta E_{2CT} - K_{xy})} \tag{6.49a}$$

and the analogous contribution to the singlet is

$$\sum_{i,j=8,10} \frac{\langle \Psi_2|\hat{H}|\Psi_i\rangle\langle\Psi_i|\hat{H}|\Psi_{12}\rangle\langle\Psi_{12}|\hat{H}|\Psi_j\rangle\langle\Psi_j|\hat{H}|\Psi_2\rangle}{-E_i \cdot E_j \cdot E_{12}}$$
$$= -\frac{16t_{pd}^4}{(\Delta E'_{CT})^2(\Delta E_{2CT} + K_{xy})} \tag{6.49b}$$

The singlet-only term is small because of the presence of t_{ab} in the numerator, and hence, the other contribution is expected to be the dominant one. This second contribution is identical for both states except for the energy of the intermediate state with two unpaired electrons on the oxygen: Ψ_{11} and Ψ_{12} for triplet and singlet, respectively. Recalling Hund's rule for the tendency towards maximum spin multiplicity of unpaired electrons on one atom makes clear that the energy of Ψ_{11} will be significantly lower than the intermediate state on the singlet path (by $2K_{xy}$ to be precise), and hence, the fourth-order correction to the energies favors the ferromagnetic alignment of the spin moments on the cations.

6.5 Spin Waves for Ferromagnets

The last part of this chapter leaves behind the local viewpoint of the electronic structure and explores the description of magnetic interactions from a periodic perspective. Let us consider a lattice with N sites. Each site has a spin angular moment of S and all spins are aligned along the principal magnetization axis ($M_S = S$), corresponding to the ground state of a set of ferromagnetically coupled centers. The Heisenberg Hamiltonian for such a lattice reads

$$\hat{H} = -\sum_{i<j} J_{ij}\left[\frac{1}{2}\left(\hat{S}^+(i)\hat{S}^-(j) + \hat{S}^-(i)\hat{S}^+(j)\right) + \hat{S}_z(i)\hat{S}_z(j)\right] \tag{6.50}$$

and the wave function is characterized by the M_S value at each lattice site

$$\Phi_0 = |S_1, S_2, \ldots, S_i, S_j, \ldots, S_N\rangle \tag{6.51}$$

To calculate the energy of Φ_0 we evaluate the effect of the different terms of the Hamiltonian separately and then add them up to obtain the energy.

$$\hat{S}^+(i)\hat{S}^-(j)|S_1, S_2, \ldots, S_i, S_j, \ldots, S_N\rangle = 0$$
$$\hat{S}^-(i)\hat{S}^+(j)|S_1, S_2, \ldots, S_i, S_j, \ldots, S_N\rangle = 0 \tag{6.52}$$
$$\hat{S}_z(i)\hat{S}_z(j)|S_1, S_2, \ldots, S_i, S_j, \ldots, S_N\rangle = S^2|S_1, S_2, \ldots, S_i, S_j, \ldots, S_N\rangle \tag{6.53}$$

The zero's in the first two contributions are due to the fact that a spin with maximum M_S-value cannot climb further on the ladder by $\hat{S}^+$. From this, we confirm that Φ_0 is an eigenfunction with eigenvalue

$$E_0 = -S^2 \sum_{i<j} J_{ij} \tag{6.54}$$

Next, we study the low-lying excitations of the ferromagnet, following Kaxiras [20]. To generate an excited state, the M_S value at one of the sites is lowered from $M_S = S$ to $S - 1$ by applying $\hat{S}^-(i)$ on Φ_0, the smallest change that can be imagined. To ensure that the excited state is also an eigenfunction of the Heisenberg Hamiltonian two determinants are needed

$$\begin{aligned} \Phi_1 &= |S_1, S_2, \ldots, S_i - 1, S_j, \ldots, S_N\rangle \\ \Phi_2 &= |S_1, S_2, \ldots, S_i, S_j - 1, \ldots, S_N\rangle \end{aligned} \tag{6.55}$$

The action of the ladder operators on such functions is defined in Eq. 1.23 and results in

$$\begin{aligned} \hat{S}^+(i)\hat{S}^-(j)\Phi_1 &= \hat{S}^+(i)\sqrt{(S+S)(S+1-S)}|S_1, S_2, \ldots, S_i - 1, S_j - 1, \ldots, S_N\rangle \\ &= \sqrt{2S}\sqrt{(S-S+1)(S+1+S-1)}|S_1, S_2, \ldots, S_i, S_j - 1, \ldots, S_N\rangle = 2S\Phi_2 \end{aligned} \tag{6.56}$$

and, similarly,

$$\begin{aligned} \hat{S}^-(i)\hat{S}^+(j)\Phi_1 &= 0 \\ \hat{S}^+(i)\hat{S}^-(j)\Phi_2 &= 0 \\ \hat{S}^-(i)\hat{S}^+(j)\Phi_2 &= 2S\Phi_1 \\ \hat{S}_z(i)\hat{S}_z(j)\Phi_1 &= (S-1)S\Phi_1 \\ \hat{S}_z(i)\hat{S}_z(j)\Phi_2 &= S(S-1)\Phi_2 \end{aligned} \tag{6.57}$$

By defining $\Psi_\pm = (\Phi_1 \pm \Phi_2)/\sqrt{2}$, eigenfunctions of the Heisenberg Hamiltonian are obtained with the following eigenvalues

$$\begin{aligned} \Psi_+ : \quad \hat{H}(\Phi_1 + \Phi_2)/\sqrt{2} &= -\sum_{i<j} J_{ij}\big(S\Phi_1 + S\Phi_2 + (S-1)S(\Phi_1 + \Phi_2)\big)/\sqrt{2} \\ &= -\sum_{i<j} J_{ij}(S + S(S-1))(\Phi_1 + \Phi_2)/\sqrt{2} = -\sum_{i<j} J_{ij}S^2\Psi_+ \end{aligned} \tag{6.58}$$

$$\Psi_- : \quad \hat{H}(\Phi_1 - \Phi_2)/\sqrt{2} = -\sum_{i<j} J_{ij}\big(-S\Phi_1 + S\Phi_2 + (S-1)S(\Phi_1 - \Phi_2)\big)/\sqrt{2}$$
$$= -\sum_{i<j} J_{ij}(-S + S^2 - S)(\Phi_1 - \Phi_2)/\sqrt{2} = -\sum_{i<j} J_{ij}(S^2 - 2S)\Psi_- \tag{6.59}$$

E_+ is identical to the ground state value and the corresponding wave function has the same spin multiplicity as Φ_0 but the total M_S value is lowered by one. The second energy, E_-, is higher than E_0 (remember that the J_{ij} are positive for a ferromagnetic system) and describes a state where the total spin moment is no longer equal to the maximum value.

6.6 Consider a system with two $S = 1$ magnetic sites. The ferromagnetic solution is $\Phi_0 = \alpha\alpha\alpha\alpha$. Check that $\Psi_\pm = (M_{S,max}, M_{S,max}-1) \pm (M_{S,max}-1, M_{S,max})$ are indeed eigenfunctions of the Heisenberg Hamiltonian and that the *plus* combination corresponds to a quintet and the *minus* combination to a triplet.

This description of the excited state does however not respect the translational symmetry of the crystal and an extra step has to be taken to obtain a more complete description. First, we change from discrete point indexation $(1, 2, \ldots i, j, \ldots, N)$ to a more convenient representation based on the distance between two lattice sites. Figure 6.16 shows how the discrete labeling of lattice sites can be replaced by a representation based on the distance r between these through the vectors $\mathbf{r}$. Although slightly more abstract, this choice is more versatile for an extended system with, in principle, infinite lattice sites and translational symmetry.

The Heisenberg Hamiltonian of Eq. 6.50 remains the same except that the indices i and j are replaced by $\mathbf{r}'$ and $\mathbf{r}''$.

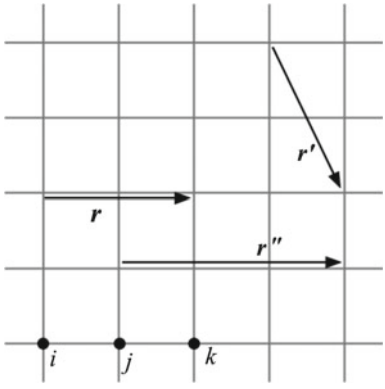

Fig. 6.16 Definition of $\mathbf{r}$, $\mathbf{r}'$ and $\mathbf{r}''$ used in the derivation of the spin wave representation of the excited states of an Heisenberg ferromagnetic extended system

$$\hat{H} = -\sum_{\mathbf{r}'<\mathbf{r}''} J(\mathbf{r}'-\mathbf{r}'')\left[\frac{1}{2}\left(\hat{S}^{+}(\mathbf{r}')\cdot\hat{S}^{-}(\mathbf{r}'')+\hat{S}^{-}(\mathbf{r}')\cdot\hat{S}^{+}(\mathbf{r}'')\right)+\hat{S}_z(\mathbf{r}')\hat{S}_z(\mathbf{r}'')\right] \tag{6.60}$$

The general expression for the excited state that respects the translational symmetry is obtained by applying the same procedure that is followed to construct the well-known Bloch functions to represent the single-particle wave functions in a crystal.

$$|\Phi_k\rangle = \sum_r e^{i\mathbf{k}\cdot\mathbf{r}}\hat{S}^{-}(\mathbf{r})|\Phi_0\rangle \tag{6.61}$$

where Φ_0 is the ferromagnetic ground state with maximum M_S-value (all spin moments aligned along the principal magnetic axis) and Φ_k a state with $M_S = M_{S,max} - 1$. We will follow the same strategy as above to determine the energy of this extended wave function by letting the Hamiltonian act on it. First, the action of $\hat{S}_z(\mathbf{r}')\hat{S}_z(\mathbf{r}'')$ on the spin dependent part of $|\Phi_k\rangle$:

$$\begin{aligned}\hat{S}_z(\mathbf{r}')\hat{S}_z(\mathbf{r}'')\hat{S}^{-}(\mathbf{r})|\Phi_0\rangle &= [S(S-1)(\delta_{\mathbf{r}'\mathbf{r}}+\delta_{\mathbf{r}''\mathbf{r}})+S^2(1-\delta_{\mathbf{r}'\mathbf{r}}-\delta_{\mathbf{r}''\mathbf{r}})]\hat{S}^{-}(\mathbf{r})|\Phi_0\rangle \\ &= (S^2 - S\delta_{\mathbf{r}'\mathbf{r}} - S\delta_{\mathbf{r}''\mathbf{r}})\hat{S}^{-}(\mathbf{r})|\Phi_0\rangle \end{aligned} \tag{6.62}$$

This expression shows that the product of two $\hat{S}_z$ operators results nearly always in S^2, except when $\mathbf{r}$ coincides with $\mathbf{r}'$ or $\mathbf{r}''$ where it acts on a spin function with an M_S-value lowered by 1, resulting in $S(S-1)$. This is conveniently represented with the Kronecker delta functions in the expression. This results leads us directly to the expression that reflects the action of the last term of the Hamiltonian on Φ_k

$$\begin{aligned}&-\sum_{\mathbf{r}'<\mathbf{r}''} J(\mathbf{r}'-\mathbf{r}'')(S^2 - S\delta_{\mathbf{r}'\mathbf{r}} - S\delta_{\mathbf{r}''\mathbf{r}})\sum_{\mathbf{r}} e^{i\mathbf{k}\cdot\mathbf{r}}\hat{S}^{-}(\mathbf{r})|\Phi_0\rangle \\ &= \left[-S^2\sum_{\mathbf{r}'<\mathbf{r}''} J(\mathbf{r}'-\mathbf{r}'') + 2S\sum_{\mathbf{r}\neq 0} J(\mathbf{r})\right]|\Phi_k\rangle = \sum_{r\neq 0}\left(-\frac{1}{2}S^2 + 2S\right)J(\mathbf{r})|\Phi_k\rangle \end{aligned} \tag{6.63}$$

The first two terms of the Hamiltonian concern the products of step-up and step-down operators

$$\begin{aligned}\hat{S}^{-}(\mathbf{r}')\hat{S}^{+}(\mathbf{r}'')\hat{S}^{-}(\mathbf{r})|\Phi_0\rangle &= 2S\delta_{\mathbf{r}\mathbf{r}''}\hat{S}^{-}(\mathbf{r}')|\Phi_0\rangle \\ \hat{S}^{+}(\mathbf{r}')\hat{S}^{-}(\mathbf{r}'')\hat{S}^{-}(\mathbf{r})|\Phi_0\rangle &= 2S\delta_{\mathbf{r}\mathbf{r}'}\hat{S}^{-}(\mathbf{r}'')|\Phi_0\rangle \end{aligned} \tag{6.64}$$

Half the sum of these two terms gives

$$\frac{1}{2}\left[\hat{S}^{-}(\mathbf{r}')\hat{S}^{+}(\mathbf{r}'')\hat{S}^{-}(\mathbf{r}) + \hat{S}^{+}(\mathbf{r}')\hat{S}^{-}(\mathbf{r}'')\hat{S}^{-}(\mathbf{r})\right]|\Phi_0\rangle = 2S\delta_{\mathbf{r}\mathbf{r}'}\hat{S}^{-}(\mathbf{r}')|\Phi_0\rangle \tag{6.65}$$

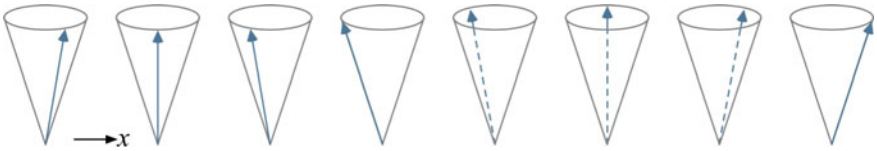

Fig. 6.17 Propagating along x of a spin wave in a one-dimensional model. The projection on the z-axis is constant ($M_{S,max} - 1$), $\langle \hat{S}_x \rangle$ and $\langle \hat{S}_y \rangle$ change from site to site

which allows us to evaluate the first terms of the Heisenberg Hamiltonian

$$
\begin{aligned}
&- \sum_{\mathbf{r}'<\mathbf{r}''} J(\mathbf{r}' - \mathbf{r}'') \sum_{r} e^{i\mathbf{k}\cdot\mathbf{r}} 2S\delta_{\mathbf{r}\mathbf{r}''} \hat{S}^-(\mathbf{r}')|\Phi_0\rangle \\
&= -2S \sum_{\mathbf{r}\neq 0} J(\mathbf{r}) e^{i\mathbf{k}\cdot\mathbf{r}} \sum_{\mathbf{r}'} e^{i\mathbf{k}\cdot\mathbf{r}'} \hat{S}^-(\mathbf{r}')|\Phi_0\rangle = -2S \sum_{\mathbf{r}\neq 0} J(\mathbf{r}) e^{i\mathbf{k}\cdot\mathbf{r}} |\Phi_k\rangle
\end{aligned}
\tag{6.66}
$$

Finally, the sum of all three terms gives the eigenvalue of $|\Phi_k\rangle$

$$
E_k = \sum_{\mathbf{r}\neq 0} \left(-\frac{1}{2} S^2 + 2S - 2Se^{i\mathbf{k}\cdot\mathbf{r}} \right) J(\mathbf{r}) = E_0 + 2S \sum_{\mathbf{r}\neq 0} (1 - e^{i\mathbf{k}\cdot\mathbf{r}}) J(\mathbf{r}) \tag{6.67}
$$

which is always higher than the ground state energy, except for $|\Phi_{k=0}\rangle$, which is degenerate with $|\Phi_0\rangle$. Figure 6.17 represents how the spin moment of $|\Phi_k\rangle$ propagates along the x-axis in a one-dimensional model. The total spin moment on each site is equal to S and the projection on the z-axis (the principal magnetic axis) is also constant, $M_{S,max} - 1$. The variation lies in the projection on the other two magnetic axes, which is easily demonstrated by calculating the expectation value of $\hat{S}_x(\mathbf{r})\hat{S}_x(\mathbf{r}') + \hat{S}_y(\mathbf{r})\hat{S}_y(\mathbf{r}')$ of $|\Phi_k\rangle$, which measures the correlation of the non-z-components of the spin moments separated by $\mathbf{r}$ and $\mathbf{r}'$.

After the usual substitution of $\hat{S}_x$ and $\hat{S}_y$ by the appropriate linear combinations of $\hat{S}^-$ and $\hat{S}^+$

$$
\langle \Phi_k | \hat{S}_x(\mathbf{r})\hat{S}_x(\mathbf{r}') + \hat{S}_y(\mathbf{r})\hat{S}_y(\mathbf{r}') | \Phi_k \rangle = \langle \Phi_k | \frac{1}{2} \left[\hat{S}^+(\mathbf{r}')\hat{S}^-(\mathbf{r}'') + \hat{S}^-(\mathbf{r}')\hat{S}^+(\mathbf{r}'') \right] | \Phi_k \rangle \tag{6.68}
$$

we evaluate the correlation function term by term

$$
\begin{aligned}
\frac{1}{2}\hat{S}^-(\mathbf{r}')\hat{S}^+(\mathbf{r}'')|\Phi_k\rangle &= \frac{1}{2} \sum_{\mathbf{r}} e^{i\mathbf{k}\cdot\mathbf{r}} \hat{S}^-(\mathbf{r}')\hat{S}^+(\mathbf{r}'')\hat{S}^-(\mathbf{r})|\Phi_0\rangle \\
&= S \sum_{\mathbf{r}} e^{i\mathbf{k}\cdot\mathbf{r}} \delta_{\mathbf{r}\mathbf{r}''} \hat{S}^-(\mathbf{r})|\Phi_0\rangle = Se^{i\mathbf{k}\cdot\mathbf{r}''} \hat{S}^-(\mathbf{r}')|\Phi_0\rangle
\end{aligned}
\tag{6.69}
$$

$$\langle \Phi_k | \frac{1}{2}\hat{S}^+(\mathbf{r}')\hat{S}^-(\mathbf{r}'') = \frac{1}{2}\hat{S}^-(\mathbf{r}'')\hat{S}^+(\mathbf{r}') \sum_{\mathbf{r}} e^{-i\mathbf{k}\cdot\mathbf{r}}\hat{S}^-|\Phi_0\rangle$$
$$= S\sum_{\mathbf{r}} e^{-i\mathbf{k}\cdot\mathbf{r}}\delta_{\mathbf{r}\mathbf{r}'}\hat{S}^-(\mathbf{r}'')|\Phi_0\rangle = Se^{-i\mathbf{k}\cdot\mathbf{r}'}\hat{S}^-(\mathbf{r}'')|\Phi_0\rangle \quad (6.70)$$

The sum of these two terms gives

$$\langle \Phi_k | \hat{S}_x(\mathbf{r})\hat{S}_x(\mathbf{r}') + \hat{S}_y(\mathbf{r})\hat{S}_y(\mathbf{r}')|\Phi_k\rangle = S(e^{-i\mathbf{k}\cdot\mathbf{r}'} + e^{i\mathbf{k}\cdot\mathbf{r}''}) = 2S\cos\left((\mathbf{r}' - \mathbf{r}'')\cdot\mathbf{k}\right) \quad (6.71)$$

showing that the orientation of the projection of the spin moment on the plane perpendicular to the principal magnetic axis varies as a cosine that depends on the separation of the spins and the lattice vector $\mathbf{k}$, exactly as the spin wave shown in Fig. 6.17.

Antiferromagnetic lattices: The description of an 'infinite' lattice with antiferromagnetic interactions is much more complicated and in fact there is no exact ground state solution for such case. The first necessary simplification towards an (approximate) description is to limit the interactions to nearest neighbours. Imagine a two-dimensional regular lattice of magnetic centers. Taking into account only nearest neighbour interactions all spins align in an anti-parallel manner. However, considering antiferromagnetic next-nearest neighbour interactions as well, the spins cannot follow the preferred alignment for centers beyond the nearest neighbours as illustrated in Fig. 6.18. This is sometimes denoted *spin frustration*. In fact, competing interactions can give rise to very interesting magnetic phenomena, and Problem 6.4 describes one of these. In the simplest case of an isolated 1D chain with only nearest neighbour antiferromagnetic interactions, an exact solution can be obtained using the Bethe ansatz.

The main problem to rigorously describe the antiferromagnetic lattice—even with the restriction of nearest neighbour interactions only—lies in the fact that the hypothetical ground state eigenfunction of the Heisenberg Hamiltonian is intrinsically multideterminantal. With increasing number of magnetic centers the

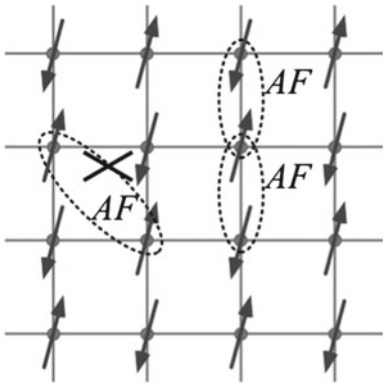

Fig. 6.18 Two-dimensional lattice of magnetic centers with antiferromagnetic nearest neighbour interactions. Next nearest neighbour antiferromagnetic interactions cannot be sustained. Note that the representation of alternating *up* and *down* spins is a simplification that is only valid for the Ising Hamiltonian

number of determinants needed to describe the antiferromagnetic state also grows. For $N = 2$, we have $\Phi_{AF} = (|\phi_1\overline{\phi}_2| - |\overline{\phi}_1\phi_2|)/\sqrt{2}$; for $N = 3$, the eigenfunction is a sum of three determinants: $\Phi_{AF} = (|2\phi_1\phi_2\overline{\phi}_3| - |\phi_1\overline{\phi}_2\phi_3| - |\overline{\phi}_1\phi_2\phi_3|)/\sqrt{6}$; and for $N = 4$, we already need a linear combination of six determinants (see Eq. 1.51). It is easy to imagine that when we consider a crystal with in principle an infinite number of magnetic sites, the wave function cannot be written down anymore.

Intuitively one could consider the state with alternating α and β spins, as drawn in Fig. 6.18, as a good representation of the ground state in an antiferromagnetic lattice. However, it is quite easy to show that this so-called Neél state is not an eigenfunction of the Heisenberg Hamiltonian and that its energy expectation value is only an upper bound to the ground state energy. Using the definition of the Heisenberg Hamiltonian given in Eq. 6.50 with $j = i + 1$ and applying periodic boundaries as mentioned in Sect. 3.3, we calculate the energy expectation value of the Neél state $\Phi_0 = |S_1, -S_2, S_3, \ldots, S_i, -S_j, \ldots - S_N|$. The action of the different products of spin operators on this function is

$$\begin{aligned} \hat{S}^+(i)\hat{S}^-(j)\Phi_0 &= 0 \\ \hat{S}^-(i)\hat{S}^+(j)\Phi_0 &= |S_1, -S_2, S_3, \ldots, S_i - 1, -S_j + 1, \ldots, -S_N| \\ \hat{S}_z(i)\hat{S}_z(j)\Phi_0 &= S^2\Phi \end{aligned} \tag{6.72}$$

This shows that Φ_0 is not an eigenfunction of the Heisenberg Hamiltonian and that the products of spin-up and spin-down operators give both zero contribution to the energy expectation value, which becomes

$$E(\Phi_0) = \frac{1}{2}NzS^2J \tag{6.73}$$

where N is the number of sites and z is the number of nearest neighbours of each magnetic center. To show that this is not the state with the lowest energy, we now generate a new spin configuration with the same total M_S value by applying the $\hat{S}^+(k)\hat{S}^-(l) + \hat{S}^-(k)\hat{S}^+(l)$ operator to the Neél state. States with different M_S values do not interact with Φ_0 and cannot lower the energy of Φ_0.

$$\begin{aligned} \Phi_1 &= (\hat{S}^+(k)\hat{S}^-(l) + \hat{S}^-(k)\hat{S}^+(l))|S_1, -S_2, S_3, \ldots S_i, -S_j, \ldots - S_N| \\ &= |S_1, -S_2, \ldots, S_k - 1, -S_l + 1, \ldots, -S_N| \end{aligned} \tag{6.74}$$

Again, we have a state that is not an eigenfunction of the Heisenberg Hamiltonian, which is easily seen by applying the products of spin-up and spin-down operators. The energy expectation value is

$$E(\Phi_1) = J\left(\frac{1}{2}zNS^2 - z + 1\right) \tag{6.75}$$

More importantly, the interaction matrix element of Φ_0 and Φ_1 is not equal to zero. Going term by term:

$$\begin{aligned}
&\langle \ldots S_i, -S_j, S_k, -S_l \ldots | -J \sum_{\langle i,j \rangle} \frac{1}{2} \hat{S}^+(i)\hat{S}^-(j) | \ldots, S_i, -S_j, S_k - 1, -S_l + 1, \ldots \rangle = -\frac{1}{2}J \\
&\langle \ldots S_i, -S_j, S_k, -S_l \ldots | -J \sum_{\langle i,j \rangle} \frac{1}{2} \hat{S}^-(i)\hat{S}^+(j) | \ldots, S_i, -S_j, S_k - 1, -S_l + 1, \ldots \rangle = 0 \\
&\langle \ldots S_i, -S_j, S_k, -S_l \ldots | -J \sum_{\langle i,j \rangle} \hat{S}_z(i)\hat{S}_z(j) | \ldots, S_i, -S_j, S_k - 1, -S_l + 1, \ldots \rangle = 0 \qquad (6.76)
\end{aligned}$$

where $\langle i, j \rangle$ symbolizes the sum over $i > j$ restricted to nearest neighbours. This non-zero matrix element means that the diagonalization of the 2×2 matrix spanned by Φ_0 and Φ_1 results in two new states, one of them with lower energy than Φ_0, showing that the Neél state is not the ground state of the antiferromagnetic lattice.

6.7 (a) Write down the wave function of the Neél state (Φ_0) for a system with 8 magnetic sites with $S = 1/2$ in its explicit form using the $\alpha(i)$ and $\beta(i)$ spin functions. (b) Calculate the energy expectation value of the Heisenberg Hamiltonian and compare to the outcome of Eq. 6.73. (c) Apply the $\hat{S}^+(3)\hat{S}^-(4) + \hat{S}^-(3)\hat{S}^+(4)$ operator on Φ_0 and calculate the expectation value of the so obtained wave function (Φ_1). (d) Calculate $\langle \Phi_0 | \hat{H} | \Phi_1 \rangle$.

Spin wave theory of antiferromagnets is a powerful method to study the ground state in these cases but goes beyond the scope of the book, the interested reader is referred to the monographs of Yosida [7] and Blundell [8].

Problems

6.1 Doublet ground state for mixed valence: Determine the magnitude of J in terms of t for which the model system defined in Fig. 6.4 has a doublet ground state.

6.2 Exchange interaction with *s*-orbital on the bridge: Consider the system depicted in Fig. 6.14 with a bridging ligand that has a *s*-orbital as outermost occupied valence orbital. Rationalize the antiferromagnetic coupling for this system.

6.3 Expectation value of a non-Neél state: Calculate the expectation value of $\Phi_1 = \hat{S}^+(i)\hat{S}^-(i+1)\Phi_0$ of the Heisenberg Hamiltonian with nearest neighbour interactions only for the following two cases: (a) Φ_0 is the Neél state of a one-dimensional chain with $N = 8$; (b) Φ_0 is the Neél state of a 4×4 lattice. Both systems have periodic boundaries and $S > \frac{1}{2}$.

6.4 Helical spin order: Consider a one dimensional spin chain with sizeable first (J_1) and second (J_2) neighbour interactions. In the mean-field approximation, the energy of the system is given by

$$E = -NS^2\big(J_1\cos(\theta) + J_2\cos(2\theta)\big)$$

In most cases the spins will align either parallel or anti-parallel, depending on the sign of J_1, but for certain ratios of J_1/J_2 spin arrangements can be observed with non-collinear spin moments. Such spin configurations are supposed to play an important role in the ferroelectric properties of magnetic materials. (a) Check that the energy expression is identical to the energy of the Neél state (Eq. 6.73) when $J_2 = 0$ and $J_1 < 0$. (b) Is there any possibility for a non-collinear alignment when $J_2 > 0$? (c) Find the three values of θ for which the energy is minimized and classify them as antiferromagnetic, ferromagnetic or non-collinear solutions. (d) Calculate the angle between two neighbouring sites with $J_2 = -0.3|J_1|$ and $J_1 = \pm 1$.

References

1. M.B. Robin, P. Day, Adv. Inorg. Chem. Radiochem. **10**, 247 (1967)
2. C. Zener, Phys. Rev. **82**(3), 403 (1951)
3. M.B. Salamon, M. Jaime, Rev. Mod. Phys. **73**, 583 (2001)
4. J.J. Girerd, V. Papaefthymiou, K.K. Surerus, E. Münck, Pure Appl. Chem. **61**, 805 (1989)
5. J.J. Borrás-Almenar, J.M. Clemente-Juan, E. Coronado, A.V. Palii, B.S. Tsukerblatt, in *Magnetism: Molecules to Materials*, ed. by J.S. Miller, M. Drillon (Wiley-VCH, 2001), pp. 155–210, chap. 5
6. P.W. Anderson, H. Hasegawa, Phys. Rev. **100**(2), 675 (1955)
7. K. Yosida, *Theory of Magnetism* (Springer, Berlin, 1996)
8. S. Blundell, *Magnetism in Condensed Matter* (Oxford University Press, Oxford, 2001)
9. W.J. Caspers, *Spin Systems* (World Scientific, Singapore, 1989)
10. J. Stöhr, H.C. Siegmann, *Magnetism: From Fundamentals to Nanoscale Dynamics* (Springer, Berlin, 2006)
11. Z. Barandiarán, L. Seijo, J. Chem. Phys. **89**, 5739 (1988)
12. K. Doll, M. Dolg, P. Fulde, H. Stoll, Phys. Rev. B **52**, 4842 (1995)
13. B. Paulus, Phys. Rep. **428**, 1 (2006)
14. V.I. Anisimov, J. Zaanen, O.K. Andersen, Phys. Rev. B **44**(3), 943 (1991)
15. L. Hedin, Phys. Rev. **139**, A796 (1965)
16. P. Fulde, H. Stoll, Found. Phys. **30**, 2049 (2000)
17. A. Stoyanova, C. Sousa, C. de Graaf, R. Broer, Int. J. Quantum Chem. **106**, 2444 (2006)
18. C. Pisani, M. Schütz, S. Casassa, D. Usvyat, L. Maschio, M. Lorenz, A. Erba, Phys. Chem. Chem. Phys. **14**, 7615 (2012)
19. E. Koch, in *Correlated Electrons: From Models to Materials*, ed. by E. Pavarini, E. Koch, M. Jarrell (Forschungszentrum Jülich GmbH Institute for Advanced Simulation, Jülich, 2012), chap. 7
20. E. Kaxiras, *Atomic and Electronic Structure of Solids* (Cambridge University Press, Cambridge, 2003)